

# The anisotropic structure of the upper mantle in the Pacific

Clyde E. Nishimura\* and Donald W. Forsyth

Department of Geological Sciences, Brown University, Providence, Rhode Island 02912, USA

Accepted 1988 July 12. Received 1988 July 12; in original form 1987 August 12

## SUMMARY

Anisotropic inversions of surface wave data show that the variations in vertical shear velocity,  $\beta_v$ , and anisotropy of the oceanic upper mantle in the Pacific are much smoother and more systematic functions of the age of the seafloor than has been reported in previous studies. The data used in this analysis are the pure-path results of previous studies on the lateral distribution of fundamental-mode Love and Rayleigh wave phase velocities (Nishimura & Forsyth 1985, 1988). The pure-path models include parameters which describe the variations with age, azimuthal anisotropy and residual depth anomalies. The calculated velocity models of the upper mantle are constrained to vary smoothly with depth and to represent the minimum deviation from an isotropic starting model. Inversions were performed using the method of Tarantola & Valette (1982).

The two best resolved parameters of the computed transversely isotropic model are the shear wave velocity terms,  $\beta_v$  and  $\xi$ . The results indicate that  $\beta_v$  above 200 km progressively increases as a function of the age of the seafloor with the pattern qualitatively mimicking isotherms of theoretical thermal cooling models. If one selects the depth to the maximum negative gradient in shear velocity as being the best available indicator of lithospheric thickness, then the thickness increases from about 15–35 km beneath 0–4 Myr old seafloor to 70–110 km in the oldest seafloor. The magnitude of the shear wave anisotropy term,  $\xi$ , rapidly increases in the first 20 Myr until some apparent constant value is reached in the older regions. A more realistic upper mantle structure is calculated using *a priori* information on the correlation between changes in shear and compressional wave velocities and the expected nature of the anisotropy. The general results are the same as the previous inversion without *a priori* constraints. Finally, the effect of attenuation is included, the primary result being an overall increase in  $\beta_v$ . The maximum change occurs at around 150 km depth, which reduces the velocity contrast between the lithosphere and asthenosphere. It is therefore more difficult to make a distinction between the plate and low-velocity zone when the effect of attenuation is included.

An estimate of the azimuthal anisotropic structure is obtained by inverting for the Rayleigh wave  $\cos 2\psi$  coefficients using derivatives calculated by the method of Montagner & Nataf (1986). The reference frame used to constrain the azimuthal effect is that of fossil seafloor spreading direction. The results indicate that in regions of the Pacific less than 80 Myr in age, there is significant anisotropy down to 200 km depth. In regions older than 80 Myr, azimuthal anisotropy is confined to the upper 50 km. The transverse and azimuthal anisotropy structures can be explained by an oceanic upper mantle containing olivine with different orientations.

**Key words:** anisotropy, surface waves, Pacific, upper mantle

## INTRODUCTION

Two forms of anisotropy are known to be present in the structure of the oceanic upper mantle. The first is that of transverse isotropy in which the elastic properties of the media differ between the horizontal and vertical orientations (Anderson 1961). This form of anisotropy is inferred from the incompatibility of fundamental-mode Love and Rayleigh

wave dispersion in an isotropic earth structure (Anderson 1966; Forsyth 1975; Schlue & Knopoff 1977; Yu & Mitchell 1979; Mitchell & Yu 1980; Journet & Jobert 1982; Regan & Anderson 1984; Yoshida 1983, 1984; Montagner 1985; Kawasaki 1986). This transversely isotropic effect has also been observed from the analysis of toroidal and spheroidal mode free oscillation data (Anderson & Dziewonski 1982). The depth to which the transverse isotropy extends into the upper mantle was initially believed to be no deeper than 220 km, although there was initially considerable debate

\* Present address: Naval Research Laboratory, Code 5110, Washington, DC 20375–5000, USA.

whether this effect was confined to either the lithosphere or asthenosphere (e.g. Schlue & Knopoff 1977; Yu & Mitchell 1979). A significant improvement in resolving the depth of this effect has been made recently by the analysis of higher-mode surface waves which have greater depth resolution than their fundamental-mode counterparts (Leveque & Cara 1983, 1985). The results of these analyses and also that of Lerner-Lam & Jordan (1983) indicate that anisotropy is present in both the lithosphere and underlying asthenosphere, and extends well into the transition region.

The other class of anisotropy which has been observed from Rayleigh wave dispersion data is dependent on the direction of wave propagation. This azimuthal anisotropic effect was initially observed by Forsyth (1975) in the Nazca plate region. Subsequent studies have shown that this effect is present in other regions of the Pacific (Yu & Mitchell 1979; Okal & Talandier 1980; Kirkwood & Crampin 1981; Montagner 1985; Cara & Leveque 1987; Suetsugu & Nakanishi 1987). Recently, we have shown that the magnitude of azimuthal anisotropy is not uniform across the Pacific but is dependent on the age of the seafloor and the period of analysis (Nishimura & Forsyth 1988). There is also an indication that this form of anisotropy is present in the Atlantic upper mantle (Kuo, Forsyth & Wyssession 1987) and on a global scale (Tanimoto & Anderson 1985). To date, no statistically required Love wave azimuthal anisotropy has been observed.

Azimuthal anisotropy was initially observed for sub-moho  $P_n$  velocities measured in marine seismic refraction studies (e.g. Hess 1964; Raitt *et al.* 1969; Keen & Barrett 1971). Later investigations have shown that the depth extent of this effect extends up into the crust (Shearer & Orcutt 1985, 1986) and down to the base of the seismic lithosphere in the western Pacific (Shimamura & Asada 1983; Shimamura 1984). While there was considerable debate concerning the exact origin of this azimuthal effect, in general the proposed models (e.g. Hess 1964; Francis 1969; Fuchs 1977; Estey & Douglas 1986) invoked the preferential alignment of olivine crystals, a highly anisotropic mineral common in the oceanic upper mantle.

In this study we solve for both the transversely and azimuthally anisotropic structure of the upper mantle in the Pacific in order to obtain a better understanding of the processes which control the evolution of the lithosphere and asthenosphere in an oceanic environment. We expect that the form of the true anisotropy in the upper mantle is not transverse with a vertical symmetry axis but more likely hexagonal or orthorhombic with horizontal symmetry. Our separate inversions for transverse and azimuthal anisotropy are intended to illustrate different aspects of the general anisotropy that are resolvable with current data. The data used are the results of our previous studies which determined the lateral distribution of fundamental-mode Love and Rayleigh wave phase velocities in the Pacific (Nishimura & Forsyth 1985, 1988). We calculate a smoothly varying transversely isotropic structure of the oceanic upper mantle that requires the minimum change from an isotropic starting model. The best resolved parameters of this analysis are the two which describe the shear wave velocities. The shear wave velocity structure calculated by this analysis shows a progressive increase in velocity as a function of the age of the seafloor down to a depth of 200 km. The

magnitude of the transversely isotropic effect in the upper 150 km is small in regions of the Pacific younger than 20 Myr in age. Transverse isotropy increases rapidly with age until some apparent constant value is reached in the older oceanic regions.

Inversions for the azimuthal anisotropic structure of the oceanic upper mantle indicate that the source of this effect extends down to about 200 km in regions of the Pacific younger than 80 Myr in age. For the oldest regions of the Pacific, azimuthal anisotropy is required only to a much shallower depth. The differences with ages may be caused by a variation in direction of the horizontal alignment of the  $a$ -axis of olivine as a function of depth rather than a diminution of intensity of anisotropy in the older Pacific.

## DATA

Fundamental-mode Rayleigh and Love wave phase velocities were recently calculated for paths which traversed the Pacific (Nishimura & Forsyth 1985, 1988) (Fig. 1). The period range for Rayleigh waves was 20–125 s, while that for Love waves was 33–125 s. In those two studies, it was determined that the velocity distributions could be modelled primarily by means of the pure-path method using a regionalization based on the age of the seafloor (Table 1; Figs 2 and 3). Additional second-order components of the velocity distributions included the effects of residual depth anomalies and Rayleigh wave azimuthal anisotropy. Azimuthal anisotropy was modelled using only the  $\cos 2\psi$  and  $\sin 2\psi$  coefficients ( $4\psi$  terms were omitted due to the lack of constraints) with the reference frame being that of fossil seafloor spreading. The best match to the observed travel-times was obtained for a model with a uniform azimuthal anisotropy effect present in oceanic regions less than 80 Myr in age. The results of the previous study also indicated that areas of the Pacific which were more than 400 m shallower than the depth predicted by the empirical age–depth curve of Parsons & Sclater (1977) were characterized by anomalously slow velocities. Shallow depth regions are believed to be created by lithospheric reheating events which represent perturbations in the normal cooling history of the oceanic plate (Crough 1978). The inclusion of a residual depth effect therefore separates oceanic regions which have not been significantly reheated (deeper seafloor depths) from regions which have been significantly altered (shallower regions). The pure-path velocities used in this study are representative of the unperturbed regions of the Pacific.

There are several advantages in using the Nishimura & Forsyth data sets in contrast to simply compiling data from the literature. First, the large number of paths used in constraining the pure-path age model produces small errors associated with the resultant pure-path velocities. This thereby provides greater constraints in our inversions. Second, the effect of azimuthal anisotropy has been taken into account and in fact the anisotropy coefficients provide additional constraints on the structure. Third, the correction for shallow residual depths results in pure-path velocities which represent the properties of ‘pristine’ oceanic plate. Fourth, the Love and Rayleigh wave data used in this study are internally consistent; they were measured and analysed by the same techniques and constraints. Finally, careful

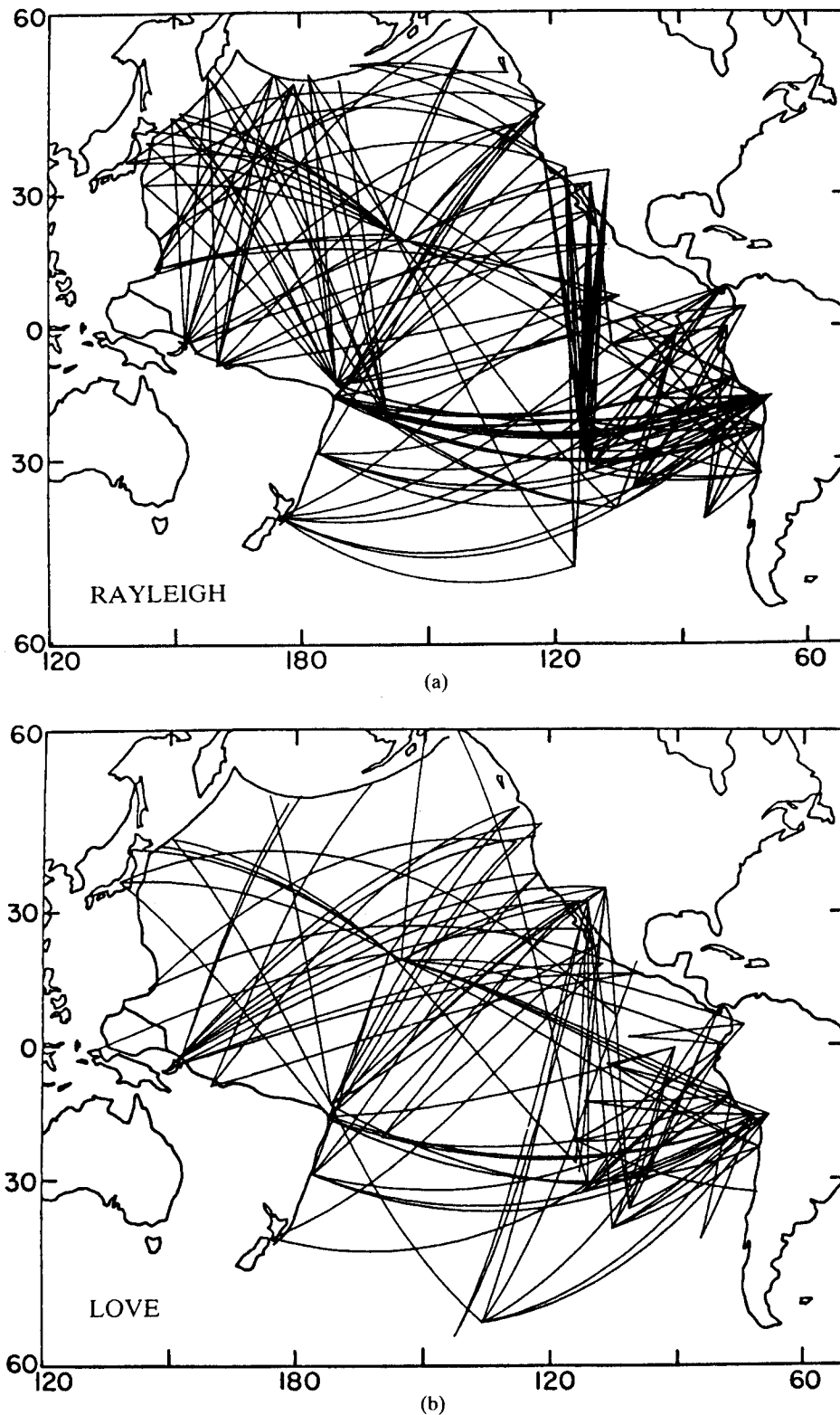


**Figure 1.** The great circle paths of (a) Rayleigh waves and (b) Love waves (Nishimura & Forsyth 1985; 1988) used to compute the pure-path velocity models of this study.

selection of higher quality data and searching for errors in source depth and mechanism has led to significantly smaller travel-time residuals than reported in most previous studies (Table 3, Nishimura & Forsyth 1985; Table 3, Nishimura & Forsyth 1988).

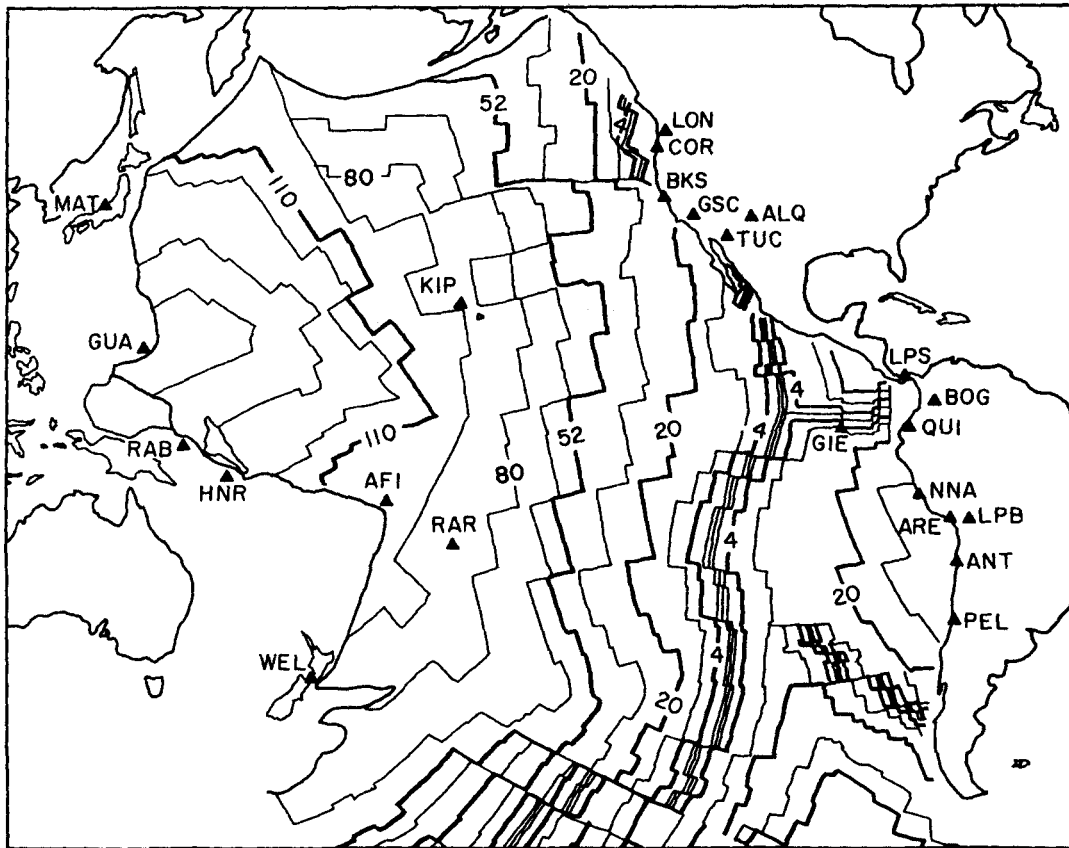
A disadvantage in this study is the omission of group velocity measurements. However, as pointed out by Knopoff & Chang (1977), group velocity measurements tend to be much noisier than those for phase velocities. As phase and group velocities provide nearly the same constraints on

**Table 1.** Observed pure-path phase velocities (left) with their associated one sigma errors (right). Values are in units of  $\text{km s}^{-1}$ .

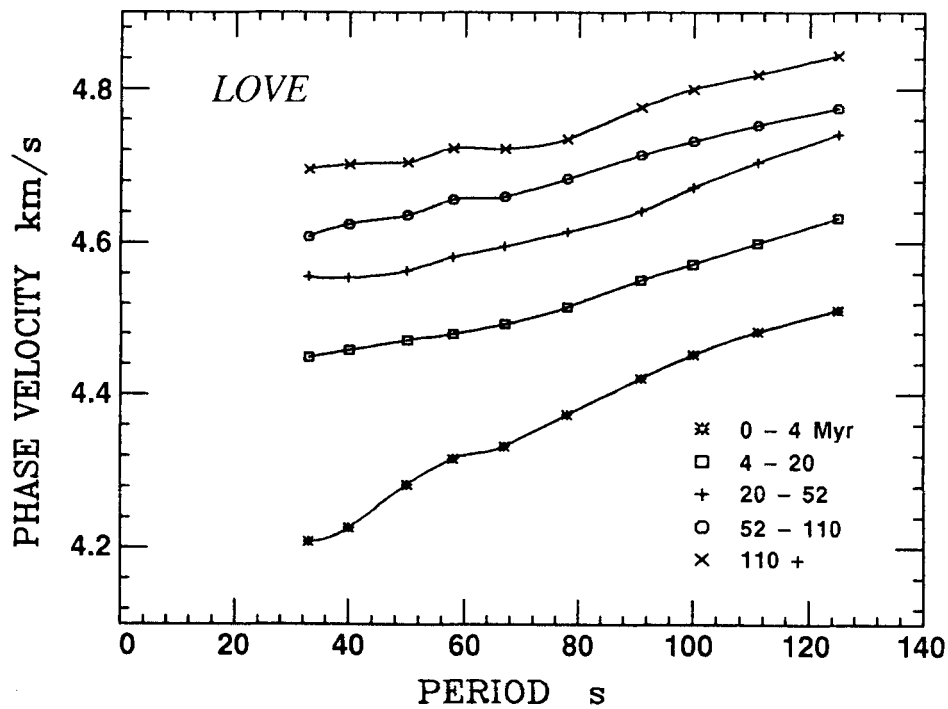
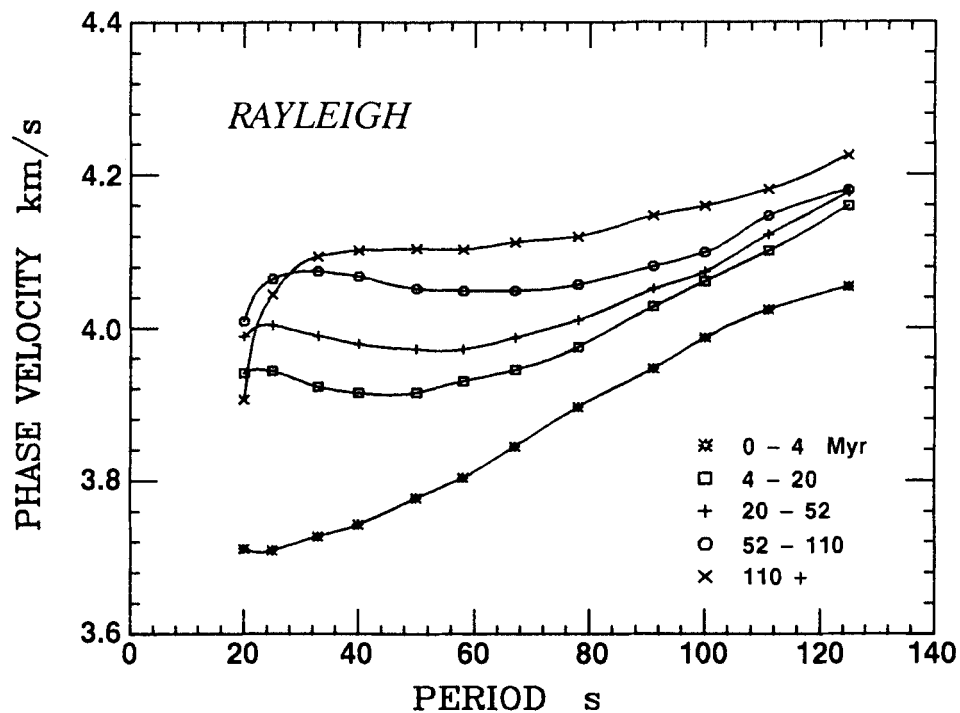
RAYLEIGH WAVE										
PURE-PATH AGE REGION (Myr)										
PERIOD	0-4		4-20		20-52		52-110		110+	
20.0 s	3.711	0.026	3.941	0.012	3.989	0.012	4.009	0.010	3.906	0.014
25.0	3.709	0.022	3.943	0.010	4.004	0.010	4.065	0.008	4.044	0.011
33.3	3.728	0.019	3.923	0.008	3.990	0.009	4.074	0.007	4.094	0.009
40.0	3.743	0.018	3.915	0.008	3.979	0.008	4.067	0.006	4.102	0.009
50.0	3.778	0.018	3.915	0.008	3.972	0.008	4.052	0.006	4.104	0.009
58.8	3.805	0.018	3.930	0.008	3.972	0.008	4.049	0.006	4.103	0.009
66.7	3.845	0.020	3.945	0.008	3.988	0.009	4.049	0.007	4.113	0.010
76.9	3.896	0.022	3.975	0.009	4.010	0.009	4.058	0.007	4.120	0.011
90.9	3.946	0.027	4.028	0.011	4.051	0.011	4.081	0.009	4.147	0.012
100.0	3.987	0.031	4.061	0.013	4.074	0.013	4.099	0.010	4.159	0.014
111.1	4.024	0.034	4.101	0.013	4.122	0.015	4.147	0.011	4.181	0.015
125.0	4.054	0.045	4.159	0.017	4.177	0.020	4.180	0.014	4.226	0.020

LOVE WAVE										
PURE-PATH AGE REGION (Myr)										
PERIOD	0-4		4-20		20-52		52-110		110 +	
33.3 s	4.208	0.026	4.449	0.011	4.556	0.016	4.608	0.011	4.696	0.019
40.0	4.226	0.024	4.458	0.010	4.554	0.015	4.624	0.010	4.702	0.018
50.0	4.282	0.024	4.471	0.010	4.563	0.015	4.636	0.010	4.705	0.017
58.8	4.316	0.024	4.479	0.010	4.581	0.014	4.656	0.010	4.723	0.017
66.7	4.332	0.025	4.492	0.010	4.595	0.015	4.660	0.010	4.722	0.017
76.9	4.373	0.026	4.515	0.011	4.614	0.015	4.683	0.011	4.735	0.018
90.9	4.421	0.028	4.551	0.011	4.641	0.016	4.714	0.011	4.776	0.019
100.0	4.452	0.029	4.572	0.012	4.672	0.017	4.732	0.012	4.800	0.020
111.1	4.482	0.032	4.599	0.013	4.705	0.019	4.753	0.013	4.819	0.022
125.0	4.511	0.036	4.632	0.015	4.741	0.021	4.775	0.014	4.844	0.025



**Figure 2.** Age of the seafloor, after Sclater *et al.* (1981), showing the age regionalization (thick lines) used in the pure-path analyses (0-4, 4-20, 20-52, 52-110, 110+ Myr). The pure-path model also included two continental-type regimes. The 80 Myr isochron used to separate two azimuthally anisotropic regions of the Pacific is also labelled. Also shown by triangles are the WWSSN seismic stations used for the surface wave observations.



**Figure 3.** Rayleigh (a) and Love (b) pure-path phase velocities used in this study to constrain the upper mantle structure. Regionalization was based on the age of the seafloor (Fig. 2) using five age regions (0–4, 4–20, 20–52, 52–110, and 110+ Myr) along with two continental-type regions (North America and South America/Island arc). The pure-path model also incorporated the effect of residual depth regions that were 400 m shallower than the depth predicted by the Parsons & Sclater (1977) age–depth curve. Rayleigh waves were also modelled using azimuthal anisotropy (fossil seafloor spreading reference frame). Two anisotropic pure-path regions were used (less than and greater than 80 Myr in age). The period range for the Rayleigh waves is 20–125 s and for Love waves 33–125 s.

the upper mantle structure (Wiggins 1972), the additional benefit of including group velocities is partially negated by the larger errors associated with group velocity calculations. Since group velocities for Love waves are particularly unreliable in this period range because of higher-mode interference (Boore 1969), we chose to measure phase velocities only for both Love and Rayleigh waves to maintain a uniform structure to the data set.

### MODEL SYMMETRY

An important factor in the inversion for an anisotropic velocity structure is the assumed symmetry system of the media. For fundamental-mode surface wave data, the most commonly assumed system used is that of transverse isotropy; a hexagonal system with a vertical axis of symmetry. The advantages of transverse isotropy are two-fold; first it is a natural system by which to model vertically polarized Rayleigh and horizontally polarized Love wave dispersion, and secondly, this system is the only anisotropic structure in which there exists an exact solution to the normal-mode problem for a spherical earth (Takeuchi & Saito 1972; Anderson & Dziewonski 1982).

On the other hand, if azimuthal dependent variations exist, then a lower symmetry model is required; the most commonly proposed being a hexagonal system with a horizontal rather than a vertical axis of symmetry (Crampin 1984; Maupin 1985; Kawasaki 1986; Estey & Douglas 1986). The primary justification for using such a symmetry system is that it describes an oceanic upper mantle which contains systematically aligned olivine crystals; in this case, with the fast olivine  $a$ -axis [100] preferentially oriented in the horizontal plane. Such a model is one that has been universally proposed as a means of explaining seismic refraction derived azimuthal anisotropy and also the results of laboratory measurements of the elastic properties of ultramafic rocks from ophiolite sequences. A hexagonal system with a horizontal axis of symmetry can also produce an apparent transversely isotropic effect for Rayleigh and Love wave dispersion if the propagation paths average out the azimuthal dependency (Fig. 4); this is the case for the computed pure-path velocities. The computed horizontal and vertical velocities of the assumed transversely isotropic

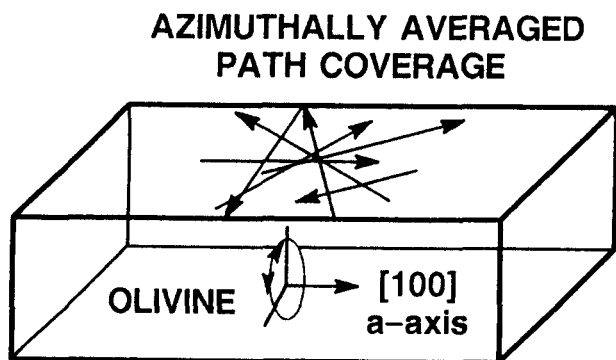


**Figure 4.** Conversion of hexagonal system with horizontal axis of symmetry to a transversely isotropic model with vertical axis of symmetry when paths average over the range of possible azimuths. The computed transversely isotropic velocities represent averages of the true velocities of the media.

media are therefore representative of the average of the true velocities (Estey & Douglas 1986).

For the purposes of this study, we will use a transversely isotropic media to model the calculated Rayleigh and Love wave pure-path phase velocities; the computed age dependent velocities are representative of azimuthally averaged values. The azimuthally dependent component of the velocity structure will then be modelled using the computed azimuthal anisotropy coefficients. If aligned olivine is the cause of the observed anisotropy then this procedure separates the anisotropic structure into two components: (i) a measure of the degree of olivine  $a$ -axis alignment in the horizontal versus vertical plane (transverse isotropy), and (ii) the amount of preferential alignment of the  $a$ -axis in the horizontal plane (azimuthal anisotropy).

### INVERSION METHOD AND MODELLING PHILOSOPHY

An inversion for a transversely isotropic structure, constrained by fundamental-mode phase velocities, represents both an underdetermined and non-linear problem. The final model is therefore highly dependent on the whims of the modeller whether it be the choice of the inverse technique, starting model and/or *a priori* constraints employed. With this freedom and the limited resolving power inherent in fundamental-mode surface wave data, one can then calculate a host of models which 'fit' the data satisfactorily.

We have inverted for the anisotropic structure of the oceanic upper mantle guided by the following philosophy.

(1) *The final model should vary smoothly as a function of depth.* When one models data with limited depth resolution, the resultant model should also reflect this limitation. From a strictly inverse modelling point of view, the smoothest varying model which deviates the least from the starting case is the model that best represents the inherent resolution of the data (Tarantola & Valette 1982). Discrete models which separate the lithosphere and asthenosphere into two distinct parameters (e.g. Schule & Knopoff 1977; Yu & Mitchell 1979; Regan & Anderson 1984; Kawasaki 1986) directly impose *a priori* constraints on the problem which may not exist from a seismological point of view and which may mislead members of the scientific community not familiar with the limitations on resolution. Thermal models have shown that there is a gradual temperature transition between the lithosphere and the asthenosphere (e.g. Parker & Oldenburg 1973; Parsons & Sclater 1977). If the elastic properties are a function of temperature, then the transition from the lithosphere to the asthenosphere will be characterized by a gradual change in the seismic velocities. On the other hand, there is a sharper distinction between mechanical properties of the lithosphere and asthenosphere based on the flexure of the oceanic plate (e.g. McNutt 1984). However, the elastic flexure thickness which is representative of the change from a brittle to ductile regime is a measure of the long-term response of the plate. Seismic waves obviously require a much shorter response time and therefore flexural and seismic calculations model two different aspects of the properties of the oceanic upper mantle.

(2) *If some a priori information is available then it should*

be incorporated into the model and not discarded. For instance, it is expected that a change in the shear wave velocity will be accompanied by a corresponding change in the compressional wave velocity. Furthermore, some general form of the anisotropy expected in the upper mantle is known from the elastic properties of mantle rocks derived from ophiolite structures; for instance it is not expected that  $\beta_H > \beta_V$  if  $\alpha_H < \alpha_V$ .

(3) Changes as a function of age of seafloor should be minimized, i.e. although details of any one model will be non-unique, the changes in the model from one age zone to another should include only those features required by the data.

Finally, (4) we require that the inversion technique be robust enough to stabilize the effects of non-linearity within the framework of an underdetermined problem.

A method which can solve non-linear, underdetermined problems, while also incorporating *a priori* knowledge, is the inverse technique of Tarantola & Valette (1982). This is a versatile, powerful inversion method which is ideally suited for the problem of modelling the anisotropic structure of the oceanic upper mantle. This technique has been previously used by Montagner & Jobert (1981) to determine the structure of the upper mantle in the Pacific, and recently by Nataf, Natanishi & Anderson (1986) on a global scale.

The inversion method of Tarantola & Valette is briefly summarized here. Given some observed data,  $\mathbf{d}$ , (in this case the pure-path phase velocities for both Love and Rayleigh waves) we can then solve for some model,  $\mathbf{p}_k$  (anisotropic earth model) given some functional relationship between the two,  $\mathbf{d} = \mathbf{g}(\mathbf{p}_k)$ . If a good estimate of the starting model,  $\mathbf{p}_0$ , is known, then the model at the  $(k + 1)$ th iteration is given by

$$\mathbf{p}_{k+1} = \mathbf{p}_0 + \mathbf{C}_{pp} \mathbf{G}_k^T (\mathbf{C}_{dd} + \mathbf{G}_k \mathbf{C}_{pp} \mathbf{G}_k^T)^{-1} \times [(\mathbf{d} - \mathbf{g}(\mathbf{p}_k) + \mathbf{G}_k(\mathbf{p}_k - \mathbf{p}_0)], \quad (1)$$

where

$\mathbf{p}_{k+1}$  = estimate of the model parameters for the  $(k + 1)$ th iteration,

$\mathbf{G}_k$  = partial derivatives of the model =  $\partial \mathbf{d} / \partial \mathbf{p}_k$ ,

$\mathbf{C}_{dd}$  = *a priori* data covariance matrix,

$\mathbf{C}_{pp}$  = *a priori* parameter covariance matrix.

The *a posteriori* covariance matrix of the parameters,  $\hat{\mathbf{C}}_{pp}$ , is given by

$$\hat{\mathbf{C}}_{pp} = \mathbf{C}_{pp} \mathbf{G}_k^T (\mathbf{C}_{dd} + \mathbf{G}_k \mathbf{C}_{pp} \mathbf{G}_k^T)^{-1} \mathbf{G}_k \mathbf{C}_{pp}. \quad (2)$$

The resolution matrix,  $\mathbf{R}$ , for a non-linear problem is not given by Tarantola & Valette. However, an expression is given for the linear problem, where

$$\mathbf{R} = \mathbf{C}_{pp} \mathbf{G}_k^T (\mathbf{C}_{dd} + \mathbf{G}_k \mathbf{C}_{pp} \mathbf{G}_k^T)^{-1} \mathbf{G}_k. \quad (3)$$

If the problem is quasi-linear, then it is expected that the resolution matrix will not vary appreciably between iterations (Nataf *et al.* 1986). This was the case for this study, and therefore (3) is believed to be a good approximation of the parameter resolution of the problem.

The technique finds the best-fitting final model which requires the smallest perturbations to the initial model. This differs from other inversion techniques (e.g. Wiggins 1972) which seek to minimize the changes with respect to the

parameters of the previous iteration. This is one of the aspects of the technique of Tarantola & Valette which helps to stabilize non-linear inversions. This inversion method is obviously dependent on the *a priori* information that one uses in the form of (1) the starting model, (2) the parameter covariance matrix, and (3) the data covariance matrix.

### Starting model

In a transversely isotropic medium, the material properties are given by five elastic constants and density,  $\rho$ , each of which are functions of depth. The elastic coefficients can be expressed by the three separate notational conventions (defined in the Appendix); (1)  $A$ ,  $C$ ,  $F$ ,  $L$  and  $N$ , (Love 1927), (2)  $\beta_V$ ,  $\beta_H$ ,  $\alpha_H$ ,  $\alpha_V$  and  $\eta$  or equivalently, (3)  $\beta_V$ ,  $\alpha_H$ ,  $\xi$ ,  $\phi$  and  $\eta$  (Takeuchi & Saito 1972). In this study we have chosen to use the third representation. The importance of selecting the proper anisotropic parameters has been discussed by Leveque & Cara (1985).

We use an isotropic oceanic mantle structure rather than an anisotropic model, as the starting model for our calculations. It is one of the purposes of this study to determine the minimum degree of anisotropy required to satisfy the fundamental-mode surface wave data within the philosophical constraints imposed on our inversions. Furthermore, discrete models which implicitly separate the lithosphere from the asthenosphere are inappropriate choices for our starting models; one of the constraints that we have imposed is that the final model vary smoothly with depth. Therefore, for the purposes of this study, an ideal choice for the starting model is the P7 model of Cara (1979) (Table 2; Fig. 5).

**Table 2.** Isotropic starting model adopted from that of Cara's P7 model (1979). Densities in the upper mantle vary as a function of age down to 125 km depth.

DEPTH km	$\rho$ gm/cm <sup>3</sup>	$\alpha$ km/s	$\beta$ km/s
15.0	3.3959	8.1938	4.5965
25.0	3.3819	8.1846	4.5851
35.0	3.3669	8.1750	4.5735
45.0	3.3530	8.1655	4.5620
55.0	3.3559	8.0987	4.5186
65.0	3.3583	8.0018	4.4584
75.0	3.3614	7.8656	4.3766
85.0	3.3650	7.7689	4.3170
95.0	3.3676	7.6854	4.2649
105.0	3.3702	7.6187	4.2221
115.0	3.3727	7.5698	4.1894
125.0	3.3754	7.5367	4.1655
135.0	3.3782	7.5195	4.1504
145.0	3.3811	7.5234	4.1470
155.0	3.3841	7.5626	4.1630
165.0	3.3870	7.6018	4.1790
175.0	3.3893	7.6862	4.2198
185.0	3.3916	7.7708	4.2605
195.0	3.3946	7.8574	4.3023
205.0	3.3987	7.9474	4.3458
215.0	3.4029	8.0376	4.3893
225.0	3.4087	8.1069	4.4212
235.0	3.4160	8.1552	4.4417
245.0	3.4234	8.2036	4.4622
255.0	3.4320	8.2389	4.4754
265.0	3.4427	8.2519	4.4766
275.0	3.4533	8.2650	4.4778
285.0	3.4640	8.2780	4.4790
295.0	3.4778	8.3145	4.4928

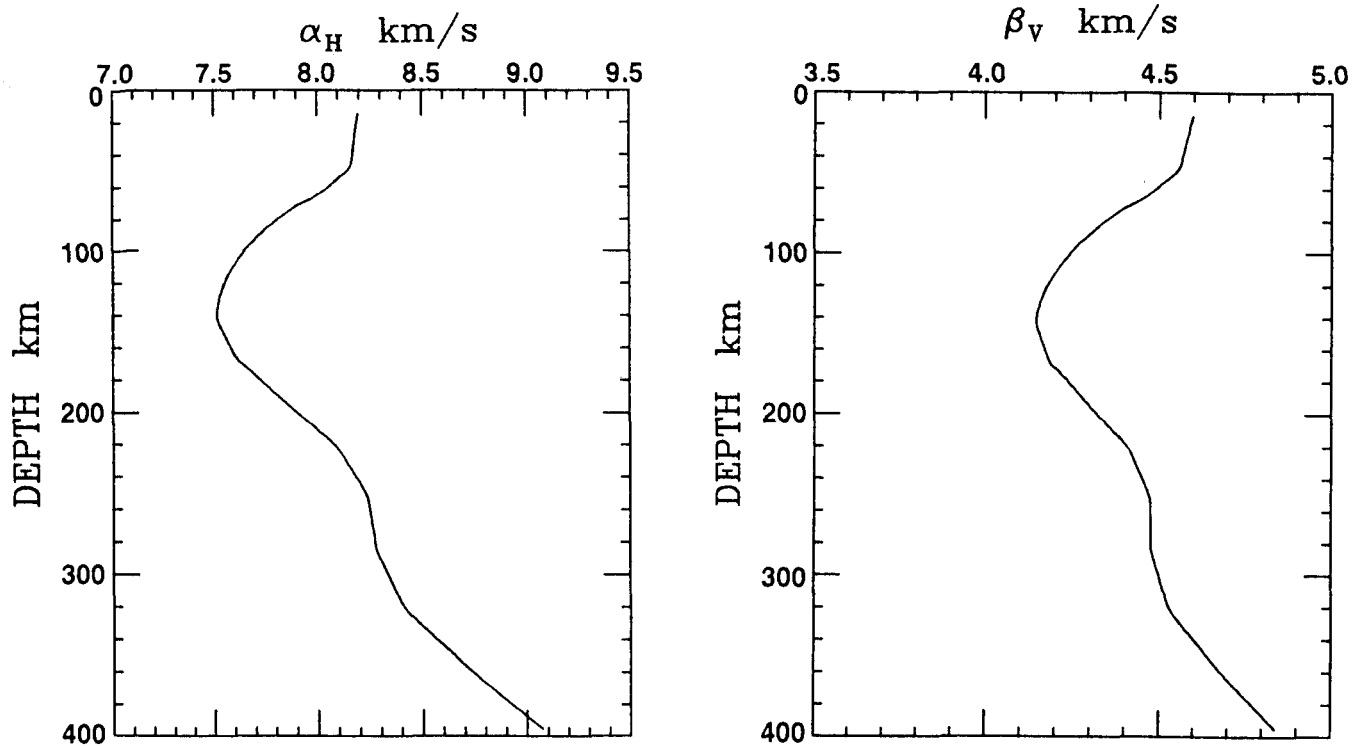


**Figure 5.** Starting isotropic model used in the calculation of the oceanic upper mantle structure with age. The shear wave velocity model is the P7 model of Cara (1979) with a modification of the compressional wave velocities. The densities are fixed parameters of the model (Fig. 6) and are dependent on the age region.

The data used to construct the P7 model were obtained from paths which traversed regions of the Pacific between 25 and 100 Myr in age. We will therefore use the results of Cara as the starting model for the 52–110 Myr age region. The calculated velocity structure for this region is then converted to an isotropic velocity structure by averaging the horizontal and vertical velocities. The isotropic structure for this region will then serve as the starting model for the adjacent age zones (20–52 and >110 Myr). This procedure of using an isotropic final model of a particular region as the starting model for the adjacent age regions applies for the remaining age zones. This satisfies the need for the starting model to be close to the final calculated model, and also the requirement that changes from one age region to the next be minimized. The calculated anisotropic structure represents the minimum degree of anisotropy required to satisfy the data.

The compressional wave velocities of the P7 model have been modified in this study so that the variations of  $\alpha$  with depth more closely mimic that of  $\beta$ . This is not critical as we will later show that  $\alpha$  is poorly resolved and hence does not affect our computed models. Furthermore, the densities were not taken to be free parameters of the inversions. Thermal calculations have clearly shown that temperature induced changes in the densities of the oceanic lithosphere caused by the effect of thermal contraction are capable of describing the variations in seafloor depth with age (Sclater, Anderson & Bell 1971; Parson & Sclater 1977). The densities of each age region (Fig. 6) were therefore assigned fixed values as predicted by some thermal structure (Parsons & Sclater 1977). Variations with depth were confined to the

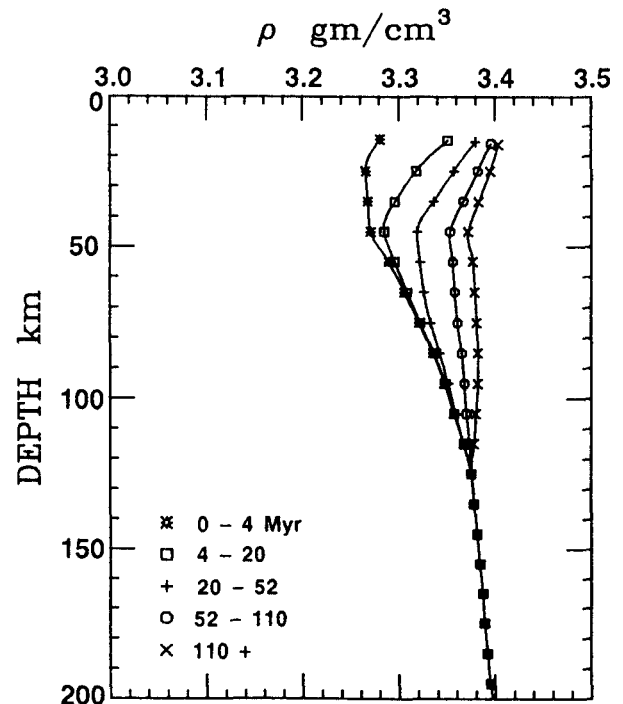


**Figure 6.** Assigned densities of the model as a function of the age region. The densities in the upper 125 km were calculated according to the predicted thermal structure of the oceanic lithosphere (Parsons & Sclater 1977). The five age regions are in isostatic equilibrium.



**Table 3.** Isotropic crustal models for the five age regions.

THICKNESS km	$\rho$ gm/cm <sup>3</sup>	$\alpha$ km/s	$\beta$ km/s	
2.90	1.03	1.50	0.00	
0.00	-	-	-	
1.00	2.60	5.60	3.30	0 - 4 Myr
2.00	2.80	6.40	3.70	
3.00	3.00	7.20	4.10	
3.65	1.03	1.50	0.00	
0.05	1.50	2.00	0.50	4 - 20 Myr
1.00	2.60	5.60	3.30	
2.00	2.80	6.40	3.70	
3.00	3.00	7.20	4.10	
4.50	1.03	1.50	0.00	
0.10	1.50	2.00	0.50	20 - 52 Myr
1.00	2.60	5.60	3.30	
2.00	2.80	6.40	3.70	
3.00	3.00	7.20	4.10	
5.50	1.03	1.50	0.00	
0.20	1.50	2.00	0.50	52 - 110 Myr
1.00	2.60	5.60	3.30	
2.00	2.80	6.40	3.70	
3.00	3.00	7.20	4.10	
6.10	1.03	1.50	0.00	
0.30	1.50	2.00	0.50	110 + Myr
1.00	2.60	5.60	3.30	
2.00	2.80	6.40	3.70	
3.00	3.00	7.20	4.10	

upper mantle above 125 km depth. Finally, the layer thickness used in this study is 10 km (except the uppermost layer), with variations in the model assumed to be confined above the 400 km seismic discontinuity (the limit of the resolving sensitivity).

The crustal structures (velocities, densities and thicknesses) of the starting model are independent of age except for variations in the water depths and sediment thicknesses (Table 3). For the purposes of this study we will assume that the crust is isotropic. Anomalous crust in the vicinity of seamounts and oceanic plateaus were accounted for in the residual depth correction applied in the calculations for the pure-path velocities. The water depths in the various age zones are the average thicknesses for a particular age region and were calculated from the empirical age–depth curves of Parsons & Sclater (1977).

#### *A priori* covariance matrix

The required *a priori* parameter covariance matrix,  $\mathbf{C}_{pp}$ , is assumed to be given by

$$C_{pp}(r_i, r_j) = s_{ij}\sigma_i\sigma_j \exp\left[\frac{(r_i - r_j)^2}{-2\Delta^2}\right], \quad (4)$$

where

$s_{ij}$  = correlation coefficient between the  $i$ th and  $j$ th parameters,

$\sigma_i$  = standard deviation of  $i$ th parameter,

$r_i$  = depth of the  $i$ th parameter,

$\Delta$  = correlation length.

A general estimate of the parameter variances,  $\sigma_i^2$ , can be made based on the results obtained from previous inversions of fundamental-mode surface wave data. The standard

deviation of the velocity structure is on the order of 0.02–0.06 km s<sup>-1</sup> (Yu & Mitchell 1979) dependent on the pure-path age region (path coverage). Since we are inverting for a complete anisotropic structure, we choose to use a conservative value of 0.05 km s<sup>-1</sup> for the errors in  $\beta_V$  and  $\alpha_H$ . The errors in the anisotropic parameters  $\xi$ ,  $\phi$  and  $\eta$  are arbitrarily taken to be 0.03. An exception to this will be applied for the youngest age region. It is known from theoretical models that there is a rapid change in the thermal properties of the upper mantle within the first few million years after accretion at the mid-ocean ridge systems. We therefore set the *a priori* error for  $\beta_V$  and  $\alpha_H$  to a larger value of 0.10 km s<sup>-1</sup> in order to allow for a greater change in velocity from the 4–20 Myr age zone to the youngest age region (0–4 Myr). The *a priori* errors for the anisotropic parameters will remain the same.

One must then choose the appropriate correlation coefficients,  $s_{ij}$ , which represent the tradeoff between the different elastic parameters and density of the model at any given depth. The covariances are given by  $\sigma_{ij} = s_{ij}\sigma_i\sigma_j$  with the selection of the appropriate correlation coefficients strongly dependent on one's personal preference. It is known that, for rocks which are representative of that found in the mantle, a change in shear wave velocity,  $\beta_V$ , is accompanied by a corresponding change in the compressional wave velocity,  $\alpha_H$ , assuming a relatively constant Poisson's ratio. Another *a priori* inference is that it is not expected that  $\beta_H > \beta_V$  if  $\alpha_H < \alpha_V$ . This *a priori* relationship, which is constrained by the results of laboratory measurements of the elastic properties of representative mantle rocks (Peselnick & Nicolas 1978; Christensen & Salisbury 1979), requires that there be a negative correlation between anisotropic terms,  $\xi$  and  $\phi$ . We therefore set the correlation coefficient for  $\beta_V$  and  $\alpha_H$  to a value of 0.5. The correlation coefficient for  $\xi$  and  $\phi$  is taken to be -0.5. These choices of values between -1 and 1 allow the changes in parameters to be different if required by the data, but  $\beta_V$  and  $\alpha_H$ , for example, will vary together if there is no constraint or requirement that they differ.

Other values of  $s_{ij}$  are zero except that  $s_{ij}$  is taken to be 1.0 if the  $i$ th and  $j$ th parameters are the same type such as  $\beta_V$  at two different depths. Then, the correlation assumed between two different depths for the same parameters depends only on the correlation length  $\Delta$ .  $\Delta$  is the normalizing factor of the Gaussian smoothing term and controls how rapidly the structure can vary as a function of depth. The application of a Gaussian window is analogous to controlling the maximum deltaness of the resolving kernels by modifying the trade-off between parameter error and resolution in a Backus & Gilbert (1968) inversion. Previous inversions have shown that there is approximately a 0.5 km s<sup>-1</sup> peak-to-peak difference in the shear wave velocity in the lithosphere and asthenosphere. Since  $\sigma_\beta$  is taken to be 0.05 km s<sup>-1</sup> and assuming variations over 100 km depth, we therefore take  $\Delta$  to be equal to 10 km, which allows quite rapid variations with depth if they are required by the data.

#### Data covariance matrix

Previous studies which have inverted fundamental-mode surface wave data have assumed that the measured phase

velocities are independent of each other. This is true if the velocities chosen are separated by a sufficiently large period interval. In our case, there is probably some interdependence between the measured phase velocities due to systematic errors in the measurement technique; the off-diagonal terms in the data covariance matrix are small but non-zero. Unfortunately, determining the correlation between periods in each region is difficult and beyond the scope of this paper. We therefore arbitrarily assume that we can neglect the correlation between the measured phase velocities and set the off-diagonal terms of data covariance matrix equal to zero. Neglecting the off-diagonal terms in this case probably reduces the resolving power of the data since the shape of the dispersion curve may be better known than the absolute level, because some errors, such as origin time of the events, are common to all periods.

## RESULTS OF THE INVERSIONS FOR STRUCTURE

Inversions are performed to obtain the transversely isotropic structure of the Pacific as a function of the age of the oceanic plate. Two cases are analysed; (1) the correlation coefficients of the parameters are all zero, and (2)  $\beta_V$  and  $\alpha_H$ , and  $\xi$  and  $\phi$ , are correlated. An ideal starting point in

which to analyse the results of this analysis is to look at the resolution matrix.

The resolving kernels for the first model ( $s_{ij} = 0, 1$ ) clearly demonstrate that the dominant parameter is  $\beta_V$  (Fig. 7) with resolution down to about 200 km. There are also significant tradeoffs between  $\beta_V$  and other parameters, particularly  $\phi$ . Not surprisingly, the second most resolvable parameter is the shear wave transverse isotropy term. The determination of  $\xi$  depends on the apparent discrepancy between Love and Rayleigh waves with the depth resolution for  $\xi$  controlled by the poorer resolution Love waves (Rayleigh waves have greater depth resolution and constrain  $\beta_V$ ). The shapes of the resolving kernels for  $\xi$  vary more smoothly with depth than those for  $\beta_V$ ; this lack of depth resolution is a well known property of Love waves.

From this simple model in which the primary *a priori* information provided are the correlation length,  $\Delta$ , of the parameter covariance matrix, and the starting model, several important observations can be made. As expected, the most resolvable parameters are the two terms associated with the shear wave velocity structure in the upper mantle. Fortunately, the tradeoff between  $\beta_V$  and  $\xi$  is not severe, although  $\xi$  itself displays poor depth resolution. On the other hand, the other parameters are either poorly resolved or demonstrate a strong correlation with the dominant

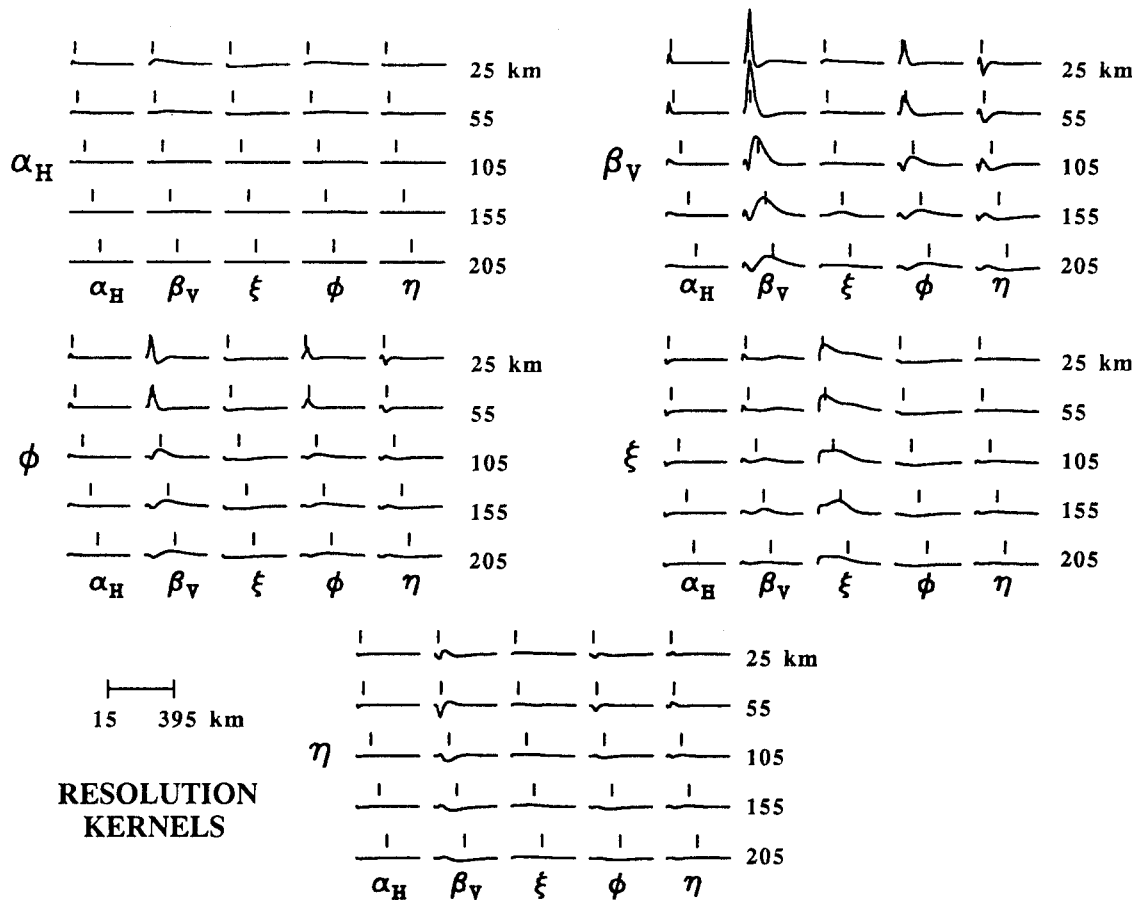


**Figure 7.** Resolution kernels for the analyses with correlation coefficients between parameters  $s_{ij} = 0, 1$  and diagonal data covariance matrix. Shown are the kernels at 25, 55, 105, 155, and 205 km depth. Tick marks are the depths where the resolving kernels are calculated. Note that  $\beta_V$  and  $\xi$  are the two most resolvable parameters with the others having either large tradeoffs with these two parameters or exhibiting little resolving power.

parameter,  $\beta_V$  (for instance,  $\phi$ ). It is therefore very difficult to delineate the amplitudes and extents of these parameters. For these reasons, we primarily focus on the two shear wave velocity parameters,  $\beta_V$  and  $\xi$ , when interpreting the results of this analysis.

The computed oceanic upper mantle structure in the five age regions are shown in Fig. 8. with the fit to the observations shown in Fig. 9. They are also given in Table 4 along with their associated errors obtained from the *a posteriori* parameter covariance matrix,  $\hat{C}_{pp}$ . A parameter is

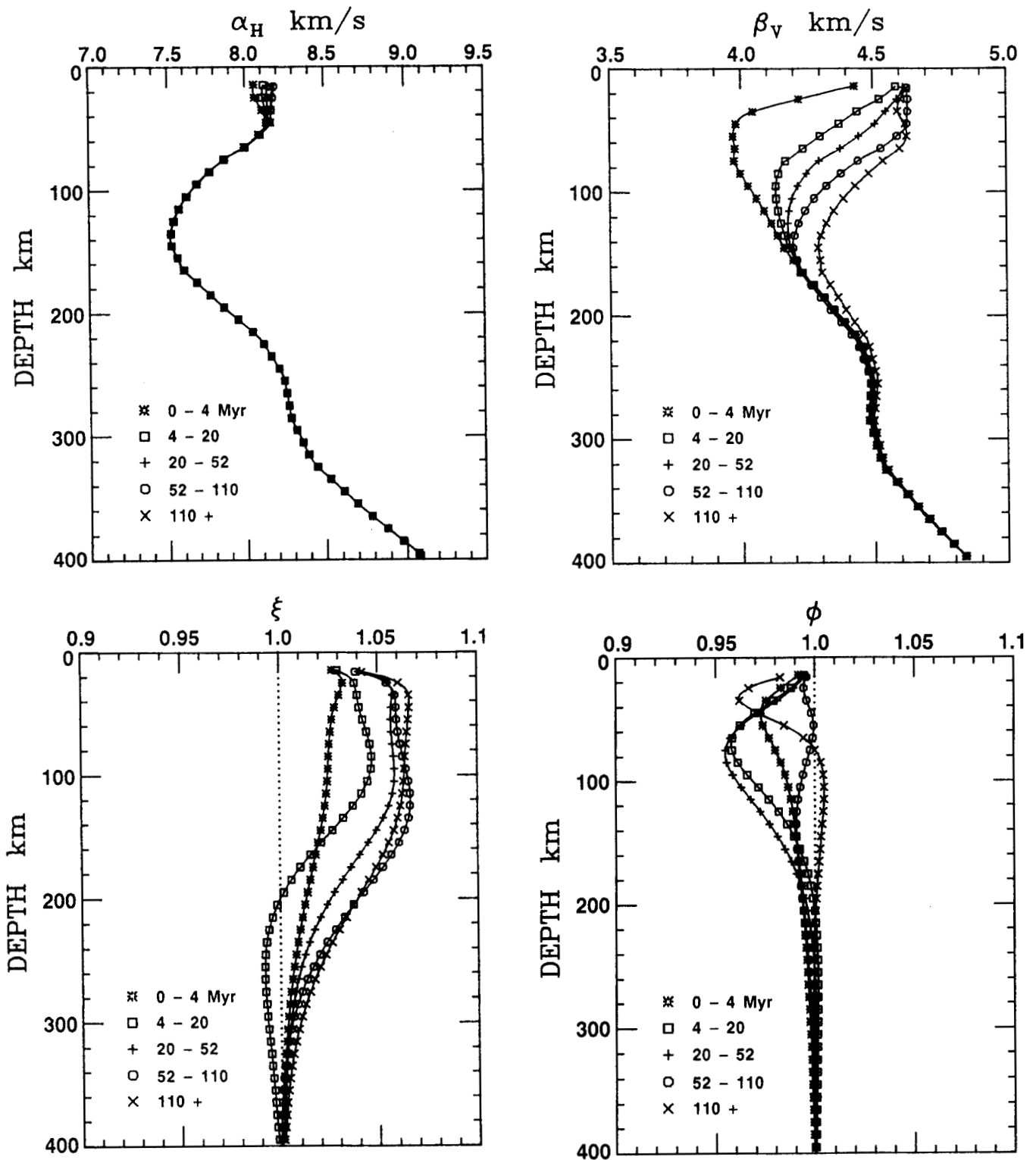


Figure 8. Calculated values of the five parameters of the inversion with  $s_{ij} = 0, 1$ . The errors are given in Table 4 and the depth resolution is shown in Fig. 7. Note the progressive increase in  $\beta_V$  with age and also the rapid increase in  $\xi$  in the first 20 Myr.

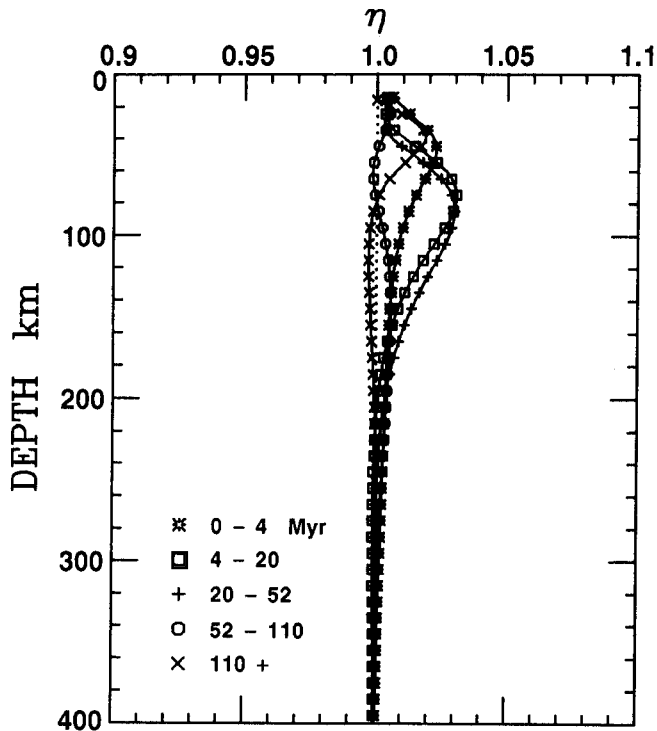


Figure 8. (Continued)

non-resolvable when the *a posteriori* variance is equal to the *a priori* variance (Tarantola & Valette 1982). Below approximately 250 km, the initial model is basically unperturbed. The dominant parameter,  $\beta_v$ , progressively increases as a function of age especially in the uppermost 100 km. This increase with age qualitatively mimics the temperature structure of oceanic lithosphere calculated by thermal cooling models with vertical heat conduction (Sclater *et al.* 1971; Parker & Oldenburg 1973). However, the results clearly show that there is no simple measure of the depth extent of the lithosphere with age. Quantification of the plate thickness using fundamental-mode surface wave data is therefore difficult and may be somewhat misleading. Although clearly a simplification, if one selects the depth to the maximum negative gradient in shear velocity as being the best available indicator of lithospheric thickness, then the thickness increases from about 15–35 km beneath 0–4 Myr old seafloor to 70–110 km in the oldest seafloor.

The anisotropic parameters also exhibit an age relationship with values of  $\xi$  rapidly increasing in magnitude above 150 km within the first 20 Myr. In the older age regions, some apparent equilibrium level is reached; there is very little variation with age. It is likely that there are variations in structure with age at depths greater than 200 km (e.g. Wielandt & Knopoff 1982; Woodhouse & Dziewonski 1984; Tanimoto 1986; Nataf *et al.* 1986). The apparent constant velocities below 200 km are due to the lack of resolving power below this depth. The initial model which was independent of age is basically unperturbed.

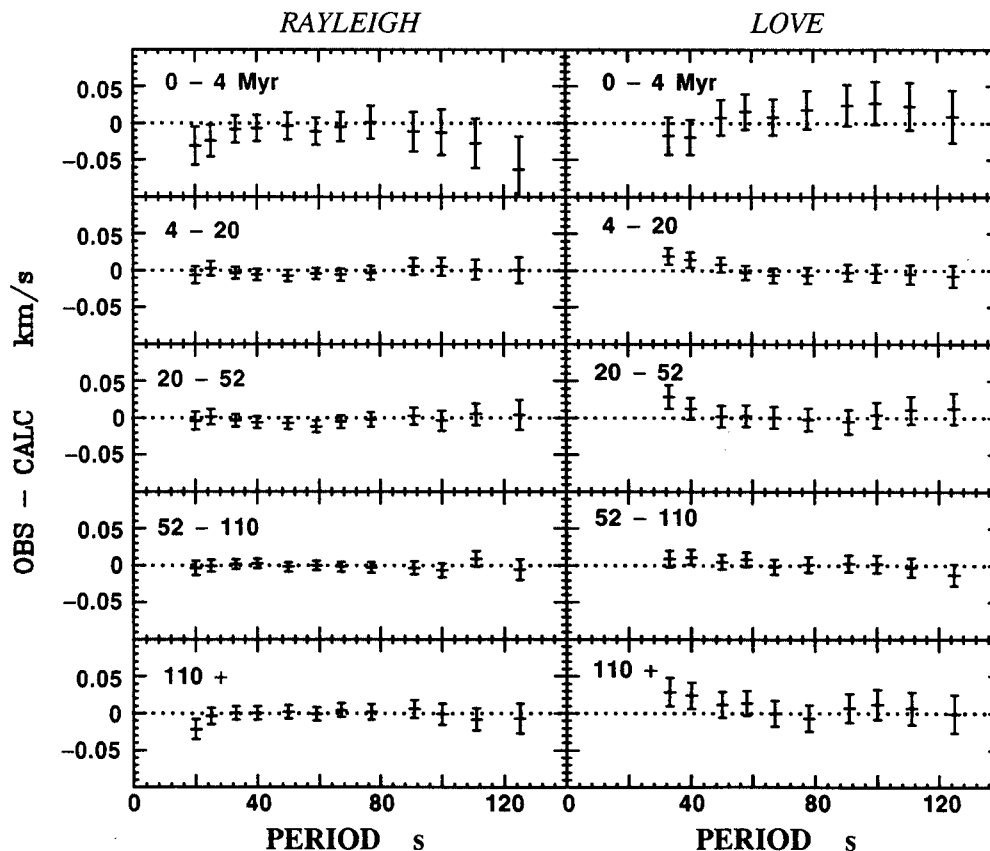


Figure 9. Fit of the model which incorporated no *a priori* information on the correlation between parameters (Fig. 8), to the observed pure-path phase velocities. Errors bars are the one sigma variations.

**Table 4.** Transversely anisotropic model for inversions with zero parameter correlation coefficients. Values on the left are the model parameters, values on the right are the one sigma errors.

REGION 1 0-4 Myr										
DEPTH km	$\alpha_H$ km/s		$\beta_V$ km/s		$\xi$		$\phi$		$\eta$	
15.0	8.0570	0.0994	4.4316	0.0849	1.0268	0.0280	0.9916	0.0299	1.0061	0.0300
25.0	8.0618	0.0995	4.2212	0.0672	1.0323	0.0269	0.9828	0.0298	1.0125	0.0299
35.0	8.1069	0.0998	4.0463	0.0646	1.0303	0.0271	0.9753	0.0296	1.0191	0.0297
45.0	8.1327	0.0999	3.9817	0.0716	1.0280	0.0273	0.9725	0.0295	1.0225	0.0297
55.0	8.0830	0.0999	3.9707	0.0762	1.0267	0.0275	0.9738	0.0295	1.0215	0.0296
65.0	7.9934	0.1000	3.9782	0.0787	1.0259	0.0278	0.9768	0.0295	1.0184	0.0297
75.0	7.8619	0.1000	3.9744	0.0808	1.0253	0.0280	0.9800	0.0296	1.0151	0.0297
85.0	7.7673	0.1000	3.9981	0.0829	1.0249	0.0283	0.9827	0.0296	1.0122	0.0298
95.0	7.6847	0.1000	4.0274	0.0850	1.0246	0.0286	0.9848	0.0297	1.0101	0.0298
105.0	7.6181	0.1000	4.0580	0.0868	1.0242	0.0288	0.9864	0.0297	1.0085	0.0299
115.0	7.5686	0.1000	4.0869	0.0883	1.0236	0.0290	0.9877	0.0297	1.0074	0.0299
125.0	7.5350	0.1000	4.1138	0.0895	1.0228	0.0292	0.9887	0.0298	1.0065	0.0299
135.0	7.5184	0.1000	4.1382	0.0905	1.0218	0.0293	0.9896	0.0298	1.0059	0.0299
145.0	7.5217	0.1000	4.1624	0.0914	1.0206	0.0294	0.9904	0.0298	1.0054	0.0299
155.0	7.5601	0.1000	4.1962	0.0921	1.0193	0.0294	0.9911	0.0298	1.0049	0.0299
165.0	7.6004	0.1000	4.2234	0.0929	1.0180	0.0295	0.9918	0.0299	1.0046	0.0300
175.0	7.6846	0.1000	4.2683	0.0936	1.0166	0.0296	0.9925	0.0299	1.0043	0.0300
185.0	7.7699	0.1000	4.3101	0.0943	1.0152	0.0296	0.9931	0.0299	1.0040	0.0300
195.0	7.8561	0.1000	4.3479	0.0949	1.0138	0.0297	0.9936	0.0299	1.0038	0.0300
205.0	7.9463	0.1000	4.3862	0.0956	1.0125	0.0297	0.9941	0.0299	1.0036	0.0300
215.0	8.0375	0.1000	4.4240	0.0962	1.0112	0.0297	0.9946	0.0299	1.0034	0.0300
225.0	8.1066	0.1000	4.4494	0.0967	1.0100	0.0298	0.9950	0.0299	1.0032	0.0300
235.0	8.1547	0.1000	4.4647	0.0972	1.0088	0.0298	0.9954	0.0299	1.0030	0.0300
245.0	8.2037	0.1000	4.4789	0.0976	1.0078	0.0299	0.9958	0.0299	1.0028	0.0300
255.0	8.2388	0.1000	4.4873	0.0980	1.0068	0.0299	0.9961	0.0300	1.0026	0.0300
265.0	8.2518	0.1000	4.4838	0.0983	1.0059	0.0299	0.9964	0.0300	1.0024	0.0300
275.0	8.2648	0.1000	4.4814	0.0986	1.0051	0.0299	0.9967	0.0300	1.0022	0.0300
285.0	8.2778	0.1000	4.4802	0.0988	1.0044	0.0299	0.9970	0.0300	1.0021	0.0300
295.0	8.3139	0.1000	4.4923	0.0990	1.0038	0.0300	0.9973	0.0300	1.0019	0.0300
305.0	8.3509	0.1000	4.5045	0.0992	1.0032	0.0300	0.9976	0.0300	1.0017	0.0300
315.0	8.3869	0.1000	4.5178	0.0994	1.0028	0.0300	0.9979	0.0300	1.0015	0.0300
325.0	8.4419	0.1000	4.5392	0.0995	1.0023	0.0300	0.9981	0.0300	1.0013	0.0300
335.0	8.5259	0.1000	4.5786	0.0996	1.0020	0.0300	0.9983	0.0300	1.0012	0.0300
345.0	8.6099	0.1000	4.6181	0.0997	1.0017	0.0300	0.9985	0.0300	1.0010	0.0300
355.0	8.6939	0.1000	4.6565	0.0998	1.0014	0.0300	0.9987	0.0300	1.0009	0.0300
365.0	8.7839	0.1000	4.6989	0.0998	1.0012	0.0300	0.9989	0.0300	1.0008	0.0300
375.0	8.8799	0.1000	4.7442	0.0999	1.0010	0.0300	0.9991	0.0300	1.0007	0.0300
385.0	8.9760	0.1000	4.7897	0.0999	1.0008	0.0300	0.9992	0.0300	1.0006	0.0300
395.0	9.0720	0.1000	4.8364	0.1000	1.0006	0.0300	0.9995	0.0300	1.0004	0.0300

REGION 2 4-20 Myr										
DEPTH km	$\alpha_H$ km/s		$\beta_V$ km/s		$\xi$		$\phi$		$\eta$	
15.0	8.1167	0.0497	4.5835	0.0453	1.0260	0.0284	0.9947	0.0298	1.0039	0.0299
25.0	8.1111	0.0497	4.5231	0.0370	1.0338	0.0272	0.9885	0.0293	1.0033	0.0298
35.0	8.1308	0.0499	4.4419	0.0339	1.0354	0.0272	0.9796	0.0291	1.0061	0.0296
45.0	8.1435	0.0499	4.3728	0.0369	1.0369	0.0274	0.9703	0.0292	1.0138	0.0296
55.0	8.0899	0.0500	4.3005	0.0393	1.0394	0.0276	0.9629	0.0293	1.0222	0.0296
65.0	7.9991	0.0500	4.2349	0.0404	1.0422	0.0277	0.9588	0.0292	1.0280	0.0295
75.0	7.8670	0.0500	4.1681	0.0412	1.0448	0.0277	0.9583	0.0292	1.0302	0.0295
85.0	7.7722	0.0500	4.1416	0.0422	1.0466	0.0277	0.9610	0.0292	1.0291	0.0296
95.0	7.6890	0.0500	4.1318	0.0430	1.0472	0.0277	0.9655	0.0293	1.0260	0.0296
105.0	7.6216	0.0500	4.1331	0.0438	1.0465	0.0278	0.9708	0.0293	1.0221	0.0297
115.0	7.5722	0.0500	4.1411	0.0444	1.0442	0.0280	0.9761	0.0294	1.0181	0.0297
125.0	7.5379	0.0500	4.1527	0.0450	1.0406	0.0283	0.9809	0.0294	1.0144	0.0298
135.0	7.5206	0.0500	4.1660	0.0455	1.0360	0.0286	0.9850	0.0295	1.0113	0.0298
145.0	7.5244	0.0500	4.1824	0.0460	1.0305	0.0288	0.9885	0.0295	1.0087	0.0298
155.0	7.5623	0.0500	4.2106	0.0464	1.0247	0.0290	0.9914	0.0295	1.0065	0.0298
165.0	7.6022	0.0500	4.2334	0.0468	1.0189	0.0292	0.9938	0.0296	1.0048	0.0299
175.0	7.6862	0.0500	4.2755	0.0471	1.0133	0.0292	0.9957	0.0296	1.0035	0.0299
185.0	7.7711	0.0500	4.3145	0.0474	1.0082	0.0293	0.9972	0.0296	1.0024	0.0299
195.0	7.8571	0.0500	4.3509	0.0476	1.0038	0.0293	0.9983	0.0297	1.0015	0.0299

Table 4. (Continued)

REGION 2 4–20 Myr										
DEPTH km	$\alpha_H$ km/s		$\beta_V$ km/s		$\xi$		$\phi$		$\eta$	
205.0	7.9471	0.0500	4.3893	0.0478	1.0002	0.0292	0.9992	0.0297	1.0009	0.0299
215.0	8.0381	0.0500	4.4267	0.0480	0.9973	0.0292	0.9999	0.0297	1.0003	0.0299
225.0	8.1070	0.0500	4.4524	0.0482	0.9951	0.0293	1.0003	0.0297	1.0000	0.0299
235.0	8.1550	0.0500	4.4675	0.0484	0.9937	0.0293	1.0007	0.0298	0.9997	0.0299
245.0	8.2040	0.0500	4.4829	0.0485	0.9928	0.0293	1.0009	0.0298	0.9995	0.0299
255.0	8.2390	0.0500	4.4917	0.0487	0.9923	0.0294	1.0010	0.0298	0.9994	0.0299
265.0	8.2520	0.0500	4.4886	0.0489	0.9922	0.0295	1.0011	0.0298	0.9993	0.0299
275.0	8.2650	0.0500	4.4868	0.0490	0.9924	0.0295	1.0011	0.0299	0.9993	0.0299
285.0	8.2780	0.0500	4.4851	0.0492	0.9927	0.0296	1.0010	0.0299	0.9993	0.0299
295.0	8.3140	0.0500	4.4975	0.0493	0.9931	0.0297	1.0010	0.0299	0.9993	0.0300
305.0	8.3510	0.0500	4.5090	0.0494	0.9936	0.0297	1.0009	0.0299	0.9993	0.0300
315.0	8.3870	0.0500	4.5225	0.0495	0.9942	0.0298	1.0009	0.0299	0.9994	0.0300
325.0	8.4420	0.0500	4.5440	0.0496	0.9947	0.0298	1.0008	0.0299	0.9994	0.0300
335.0	8.5260	0.0500	4.5825	0.0497	0.9953	0.0299	1.0007	0.0300	0.9995	0.0300
345.0	8.6100	0.0500	4.6221	0.0497	0.9958	0.0299	1.0006	0.0300	0.9996	0.0300
355.0	8.6940	0.0500	4.6596	0.0498	0.9963	0.0299	1.0005	0.0300	0.9996	0.0300
365.0	8.7840	0.0500	4.7021	0.0498	0.9967	0.0299	1.0005	0.0300	0.9997	0.0300
375.0	8.8800	0.0500	4.7465	0.0499	0.9971	0.0299	1.0004	0.0300	0.9997	0.0300
385.0	8.9760	0.0500	4.7921	0.0499	0.9976	0.0300	1.0003	0.0300	0.9998	0.0300
395.0	9.0720	0.0500	4.8380	0.0500	0.9984	0.0300	1.0002	0.0300	0.9998	0.0300

REGION 3 20–52 Myr										
DEPTH km	$\alpha_H$ km/s		$\beta_V$ km/s		$\xi$		$\phi$		$\eta$	
15.0	8.1468	0.0497	4.6146	0.0463	1.0410	0.0287	0.9945	0.0297	1.0064	0.0299
25.0	8.1381	0.0497	4.5908	0.0383	1.0547	0.0277	0.9892	0.0292	1.0036	0.0298
35.0	8.1450	0.0498	4.5485	0.0342	1.0568	0.0275	0.9811	0.0290	1.0033	0.0297
45.0	8.1490	0.0499	4.5084	0.0368	1.0562	0.0277	0.9714	0.0292	1.0092	0.0297
55.0	8.0907	0.0500	4.4468	0.0392	1.0560	0.0278	0.9631	0.0294	1.0174	0.0297
65.0	7.9983	0.0500	4.3778	0.0404	1.0563	0.0279	0.9574	0.0294	1.0243	0.0297
75.0	7.8652	0.0500	4.2970	0.0413	1.0569	0.0280	0.9550	0.0294	1.0284	0.0297
85.0	7.7700	0.0500	4.2486	0.0422	1.0577	0.0280	0.9556	0.0293	1.0297	0.0297
95.0	7.6872	0.0500	4.2145	0.0431	1.0582	0.0280	0.9585	0.0293	1.0286	0.0297
105.0	7.6200	0.0500	4.1927	0.0439	1.0582	0.0280	0.9627	0.0294	1.0262	0.0297
115.0	7.5707	0.0500	4.1813	0.0444	1.0574	0.0281	0.9675	0.0294	1.0230	0.0297
125.0	7.5373	0.0500	4.1774	0.0450	1.0556	0.0282	0.9723	0.0294	1.0197	0.0298
135.0	7.5200	0.0500	4.1791	0.0454	1.0529	0.0284	0.9768	0.0295	1.0164	0.0298
145.0	7.5237	0.0500	4.1881	0.0459	1.0495	0.0286	0.9810	0.0295	1.0135	0.0298
155.0	7.5625	0.0500	4.2126	0.0463	1.0455	0.0288	0.9846	0.0295	1.0110	0.0298
165.0	7.6023	0.0500	4.2330	0.0468	1.0411	0.0291	0.9878	0.0296	1.0088	0.0299
175.0	7.6862	0.0500	4.2758	0.0472	1.0366	0.0292	0.9905	0.0296	1.0069	0.0299
185.0	7.7712	0.0500	4.3155	0.0475	1.0322	0.0293	0.9927	0.0297	1.0054	0.0299
195.0	7.8571	0.0500	4.3537	0.0478	1.0280	0.0294	0.9945	0.0297	1.0041	0.0299
205.0	7.9471	0.0500	4.3938	0.0481	1.0242	0.0295	0.9959	0.0297	1.0031	0.0299
215.0	8.0381	0.0500	4.4322	0.0483	1.0207	0.0295	0.9970	0.0297	1.0023	0.0299
225.0	8.1070	0.0500	4.4593	0.0485	1.0176	0.0295	0.9979	0.0298	1.0017	0.0299
235.0	8.1550	0.0500	4.4751	0.0486	1.0150	0.0296	0.9986	0.0298	1.0012	0.0299
245.0	8.2040	0.0500	4.4908	0.0488	1.0127	0.0296	0.9991	0.0298	1.0008	0.0299
255.0	8.2390	0.0500	4.4996	0.0489	1.0107	0.0296	0.9995	0.0298	1.0005	0.0299
265.0	8.2520	0.0500	4.4974	0.0491	1.0090	0.0297	0.9998	0.0299	1.0003	0.0299
275.0	8.2650	0.0500	4.4953	0.0492	1.0076	0.0297	1.0000	0.0299	1.0001	0.0299
285.0	8.2780	0.0500	4.4933	0.0493	1.0064	0.0297	1.0002	0.0299	1.0000	0.0300
295.0	8.3140	0.0500	4.5054	0.0494	1.0054	0.0298	1.0003	0.0299	0.9999	0.0300
305.0	8.3510	0.0500	4.5165	0.0495	1.0046	0.0298	1.0003	0.0299	0.9998	0.0300
315.0	8.3870	0.0500	4.5287	0.0496	1.0039	0.0298	1.0004	0.0299	0.9998	0.0300
325.0	8.4420	0.0500	4.5500	0.0497	1.0033	0.0299	1.0004	0.0300	0.9998	0.0300
335.0	8.5260	0.0500	4.5883	0.0497	1.0029	0.0299	1.0004	0.0300	0.9997	0.0300
345.0	8.6100	0.0500	4.6267	0.0498	1.0025	0.0299	1.0004	0.0300	0.9998	0.0300
355.0	8.6940	0.0500	4.6641	0.0498	1.0021	0.0299	1.0004	0.0300	0.9998	0.0300
365.0	8.7840	0.0500	4.7057	0.0499	1.0019	0.0299	1.0003	0.0300	0.9998	0.0300
375.0	8.8800	0.0500	4.7502	0.0499	1.0016	0.0300	1.0003	0.0300	0.9998	0.0300
385.0	8.9760	0.0500	4.7947	0.0499	1.0013	0.0300	1.0003	0.0300	0.9998	0.0300
395.0	9.0720	0.0500	4.8399	0.0500	1.0009	0.0300	1.0002	0.0300	0.9999	0.0300

Table 4. (Continued)

REGION 4 52–110 Myr										
DEPTH km	$\alpha_H$ km/s		$\beta_V$ km/s		$\xi$		$\phi$		$\eta$	
15.0	8.1862	0.0496	4.6294	0.0465	1.0401	0.0289	0.9956	0.0295	1.0039	0.0299
25.0	8.1760	0.0496	4.6326	0.0380	1.0563	0.0278	0.9941	0.0286	1.0049	0.0298
35.0	8.1680	0.0498	4.6315	0.0332	1.0607	0.0274	0.9954	0.0284	1.0034	0.0296
45.0	8.1604	0.0499	4.6293	0.0359	1.0610	0.0275	0.9978	0.0290	1.0008	0.0297
55.0	8.0951	0.0499	4.5909	0.0381	1.0611	0.0276	0.9990	0.0294	0.9991	0.0298
65.0	7.9994	0.0500	4.5303	0.0393	1.0616	0.0279	0.9987	0.0295	0.9988	0.0298
75.0	7.8640	0.0500	4.4447	0.0404	1.0624	0.0280	0.9973	0.0296	0.9996	0.0298
85.0	7.7678	0.0500	4.3804	0.0416	1.0635	0.0281	0.9956	0.0296	1.0009	0.0298
95.0	7.6846	0.0500	4.3242	0.0427	1.0648	0.0281	0.9939	0.0295	1.0023	0.0298
105.0	7.6182	0.0500	4.2785	0.0435	1.0658	0.0280	0.9925	0.0295	1.0035	0.0298
115.0	7.5694	0.0500	4.2438	0.0441	1.0663	0.0279	0.9915	0.0295	1.0045	0.0298
125.0	7.5364	0.0500	4.2185	0.0446	1.0659	0.0279	0.9909	0.0295	1.0051	0.0298
135.0	7.5193	0.0500	4.2020	0.0450	1.0646	0.0279	0.9907	0.0295	1.0054	0.0298
145.0	7.5232	0.0500	4.1969	0.0454	1.0624	0.0280	0.9908	0.0295	1.0055	0.0298
155.0	7.5625	0.0500	4.2106	0.0458	1.0591	0.0282	0.9911	0.0295	1.0054	0.0298
165.0	7.6017	0.0500	4.2237	0.0462	1.0551	0.0285	0.9916	0.0295	1.0052	0.0298
175.0	7.6861	0.0500	4.2610	0.0466	1.0506	0.0288	0.9923	0.0296	1.0049	0.0298
185.0	7.7707	0.0500	4.2977	0.0470	1.0457	0.0290	0.9930	0.0296	1.0046	0.0299
195.0	7.8574	0.0500	4.3352	0.0474	1.0406	0.0292	0.9937	0.0296	1.0042	0.0299
205.0	7.9474	0.0500	4.3744	0.0477	1.0356	0.0294	0.9944	0.0296	1.0038	0.0299
215.0	8.0376	0.0500	4.4137	0.0479	1.0308	0.0295	0.9950	0.0297	1.0034	0.0299
225.0	8.1069	0.0500	4.4417	0.0481	1.0263	0.0295	0.9956	0.0297	1.0031	0.0299
235.0	8.1552	0.0500	4.4586	0.0483	1.0222	0.0295	0.9961	0.0297	1.0028	0.0299
245.0	8.2036	0.0500	4.4759	0.0484	1.0185	0.0295	0.9966	0.0297	1.0025	0.0299
255.0	8.2389	0.0500	4.4863	0.0486	1.0153	0.0296	0.9970	0.0298	1.0022	0.0299
265.0	8.2519	0.0500	4.4851	0.0487	1.0124	0.0296	0.9974	0.0298	1.0019	0.0299
275.0	8.2650	0.0500	4.4843	0.0488	1.0100	0.0296	0.9978	0.0298	1.0016	0.0299
285.0	8.2780	0.0500	4.4838	0.0490	1.0079	0.0296	0.9981	0.0298	1.0014	0.0299
295.0	8.3145	0.0500	4.4961	0.0491	1.0061	0.0297	0.9984	0.0299	1.0012	0.0299
305.0	8.3509	0.0500	4.5087	0.0492	1.0046	0.0297	0.9986	0.0299	1.0010	0.0299
315.0	8.3875	0.0500	4.5216	0.0493	1.0034	0.0297	0.9988	0.0299	1.0009	0.0300
325.0	8.4418	0.0500	4.5441	0.0494	1.0024	0.0298	0.9990	0.0299	1.0007	0.0300
335.0	8.5258	0.0500	4.5827	0.0495	1.0016	0.0298	0.9992	0.0299	1.0006	0.0300
345.0	8.6100	0.0500	4.6215	0.0496	1.0009	0.0298	0.9993	0.0299	1.0005	0.0300
355.0	8.6944	0.0500	4.6604	0.0497	1.0004	0.0298	0.9994	0.0300	1.0004	0.0300
365.0	8.7844	0.0500	4.7022	0.0497	1.0001	0.0299	0.9995	0.0300	1.0003	0.0300
375.0	8.8802	0.0500	4.7472	0.0498	0.9998	0.0299	0.9996	0.0300	1.0003	0.0300
385.0	8.9762	0.0500	4.7923	0.0498	0.9996	0.0299	0.9997	0.0300	1.0002	0.0300
395.0	9.0723	0.0500	4.8377	0.0499	0.9997	0.0300	0.9998	0.0300	1.0001	0.0300

REGION 5 110+ Myr										
DEPTH km	$\alpha_H$ km/s		$\beta_V$ km/s		$\xi$		$\phi$		$\eta$	
15.0	8.1763	0.0496	4.6292	0.0472	1.0429	0.0291	0.9826	0.0295	1.0000	0.0299
25.0	8.1699	0.0496	4.6051	0.0398	1.0613	0.0282	0.9666	0.0283	1.0094	0.0297
35.0	8.1677	0.0497	4.5947	0.0349	1.0665	0.0279	0.9620	0.0280	1.0176	0.0295
45.0	8.1618	0.0499	4.6222	0.0369	1.0666	0.0279	0.9712	0.0287	1.0169	0.0296
55.0	8.0964	0.0499	4.6279	0.0390	1.0660	0.0279	0.9843	0.0292	1.0109	0.0298
65.0	7.9996	0.0500	4.6022	0.0402	1.0653	0.0280	0.9943	0.0294	1.0050	0.0298
75.0	7.8641	0.0500	4.5381	0.0413	1.0646	0.0281	1.0001	0.0295	1.0010	0.0298
85.0	7.7679	0.0500	4.4856	0.0424	1.0640	0.0282	1.0030	0.0296	0.9988	0.0299
95.0	7.6848	0.0500	4.4345	0.0434	1.0635	0.0283	1.0043	0.0296	0.9977	0.0299
105.0	7.6178	0.0500	4.3893	0.0441	1.0630	0.0284	1.0047	0.0296	0.9971	0.0299
115.0	7.5688	0.0500	4.3525	0.0447	1.0623	0.0284	1.0046	0.0296	0.9970	0.0299
125.0	7.5358	0.0500	4.3239	0.0452	1.0612	0.0285	1.0043	0.0296	0.9971	0.0299
135.0	7.5188	0.0500	4.3031	0.0456	1.0596	0.0285	1.0038	0.0296	0.9973	0.0299
145.0	7.5228	0.0500	4.2923	0.0460	1.0575	0.0286	1.0032	0.0296	0.9976	0.0299
155.0	7.5618	0.0500	4.2997	0.0464	1.0548	0.0288	1.0027	0.0296	0.9980	0.0299
165.0	7.6018	0.0500	4.3056	0.0467	1.0517	0.0289	1.0021	0.0296	0.9983	0.0299
175.0	7.6859	0.0500	4.3361	0.0471	1.0482	0.0291	1.0016	0.0297	0.9987	0.0299
185.0	7.7709	0.0500	4.3655	0.0475	1.0445	0.0292	1.0011	0.0297	0.9990	0.0299
195.0	7.8569	0.0500	4.3951	0.0478	1.0406	0.0293	1.0007	0.0297	0.9993	0.0299
205.0	7.9469	0.0500	4.4280	0.0480	1.0367	0.0294	1.0003	0.0297	0.9995	0.0299
215.0	8.0379	0.0500	4.4603	0.0483	1.0328	0.0295	1.0000	0.0298	0.9998	0.0299
225.0	8.1069	0.0500	4.4823	0.0485	1.0292	0.0296	0.9997	0.0298	1.0000	0.0299
235.0	8.1549	0.0500	4.4938	0.0487	1.0257	0.0296	0.9995	0.0298	1.0001	0.0299
245.0	8.2040	0.0500	4.5059	0.0488	1.0225	0.0297	0.9994	0.0298	1.0003	0.0299
255.0	8.2390	0.0500	4.5116	0.0489	1.0196	0.0297	0.9992	0.0298	1.0004	0.0299
265.0	8.2520	0.0500	4.5068	0.0491	1.0170	0.0297	0.9991	0.0298	1.0005	0.0299
275.0	8.2650	0.0500	4.5025	0.0492	1.0146	0.0298	0.9991	0.0299	1.0005	0.0299

Table 4. (Continued)

REGION 5 110+ Myr										
DEPTH km	$\alpha_H$ km/s		$\beta_V$ km/s		$\xi$		$\phi$		$\eta$	
285.0	8.2780	0.0500	4.4986	0.0493	1.0124	0.0298	0.9991	0.0299	1.0006	0.0299
295.0	8.3140	0.0500	4.5092	0.0494	1.0106	0.0298	0.9990	0.0299	1.0006	0.0300
305.0	8.3510	0.0500	4.5190	0.0495	1.0089	0.0298	0.9991	0.0299	1.0006	0.0300
315.0	8.3870	0.0500	4.5302	0.0496	1.0075	0.0299	0.9991	0.0299	1.0006	0.0300
325.0	8.4420	0.0500	4.5507	0.0496	1.0062	0.0299	0.9991	0.0299	1.0006	0.0300
335.0	8.5260	0.0500	4.5884	0.0497	1.0052	0.0299	0.9992	0.0300	1.0005	0.0300
345.0	8.6100	0.0500	4.6263	0.0498	1.0043	0.0299	0.9992	0.0300	1.0005	0.0300
355.0	8.6940	0.0500	4.6634	0.0498	1.0036	0.0299	0.9993	0.0300	1.0005	0.0300
365.0	8.7840	0.0500	4.7047	0.0498	1.0029	0.0299	0.9994	0.0300	1.0004	0.0300
375.0	8.8800	0.0500	4.7491	0.0499	1.0024	0.0299	0.9994	0.0300	1.0004	0.0300
385.0	8.9760	0.0500	4.7936	0.0499	1.0019	0.0300	0.9995	0.0300	1.0003	0.0300
395.0	9.0720	0.0500	4.8390	0.0500	1.0013	0.0300	0.9997	0.0300	1.0002	0.0300

Obviously, it is possible to construct other models resulting in equally good fits to the observations. However, this would require relaxing the constraints of this study and would represent a change in the basic modelling philosophy. For instance Love waves are not affected at all by  $\alpha_H$ ,  $\phi$  or  $\eta$ . These parameters can then be freely manipulated with respect to the Love wave data, thereby producing a highly anisotropic structure (e.g. Regan & Anderson 1984). However, it is the difference between the Love and Rayleigh wave dispersion which required transverse isotropy.

In the second set of inversions, we use an *a priori* parameter covariance matrix which incorporates the

expected correlations of  $\alpha_H$  with  $\beta_V$ , and  $\xi$  with  $\phi$ . The results of this set of inversions produce a more 'realistic' anisotropic structure of the oceanic mantle. However, any interpretation of the results of this analysis must be made while considering the assumptions inherent in the modelling procedure.

The resolution kernels of this analysis (Fig. 10) are similar to those obtained previously except where the additional *a priori* correlation between parameters is important. This change is most apparent for  $\alpha_H$ , in which there are now large tradeoffs with the other parameters, mimicking that for  $\beta_V$  although  $\alpha_H$  itself is still poorly resolved. Likewise, the curves for  $\phi$  are also modified to take into account the

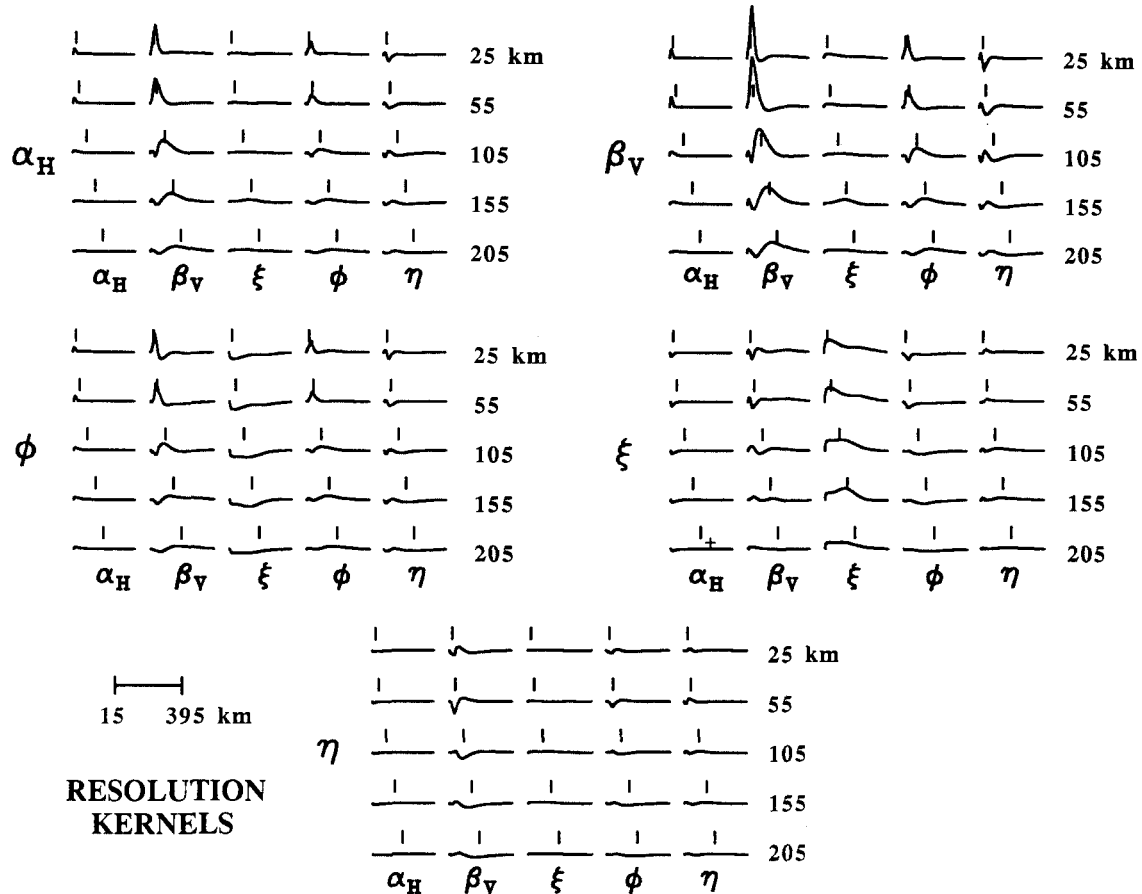
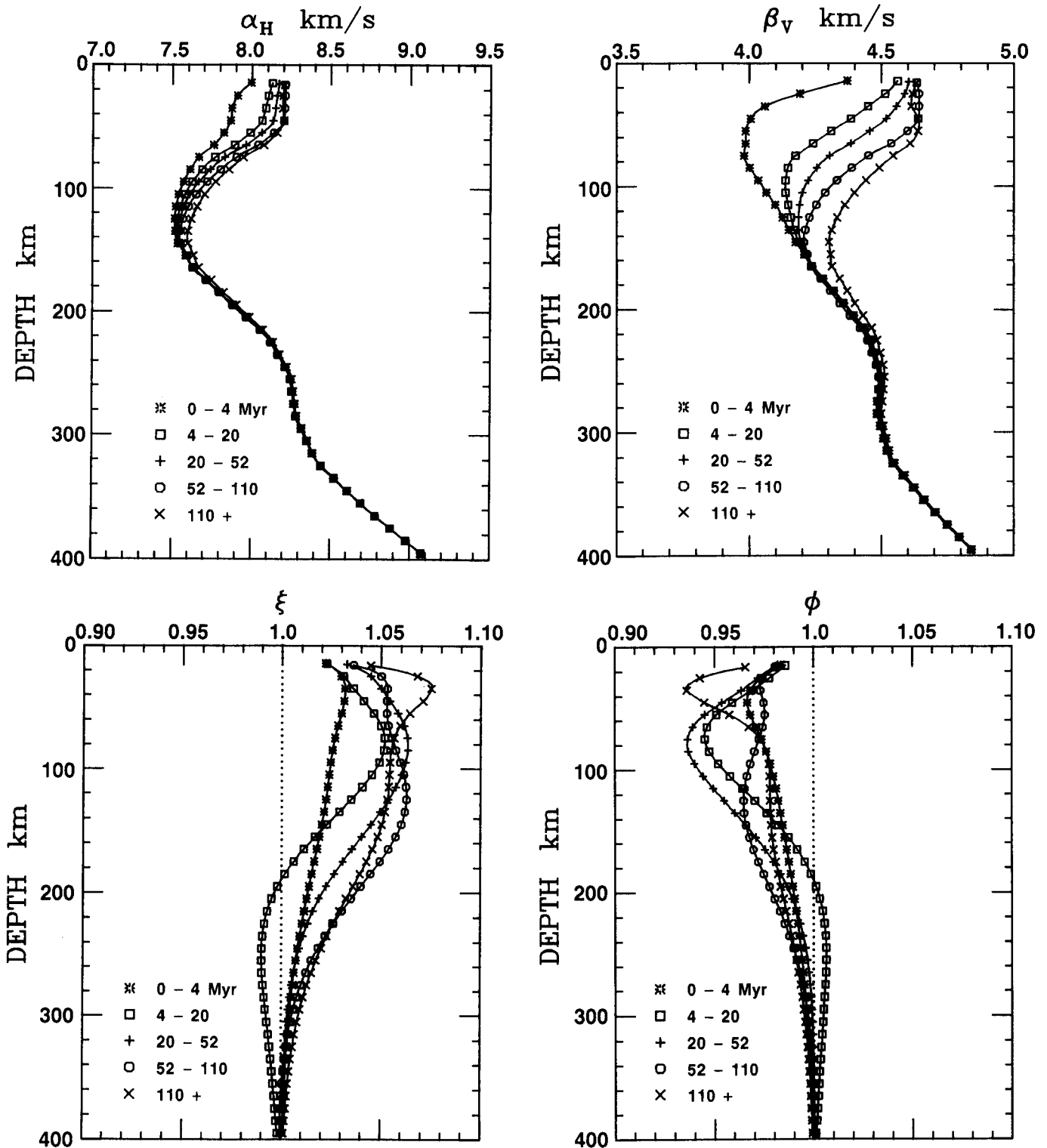


Figure 10. Resolving kernels for the model which included the correlation between  $\alpha_H$  with  $\beta_V$ , and  $\xi$  with  $\phi$ . Due to the correlation between the aforementioned parameters, there are now large off-diagonal terms compared to that of Fig. 7.



tradeoff with  $\xi$ . The values for the two dominant parameters,  $\beta_V$ , and  $\xi$ , are essentially the same for this inversion (Fig. 11) compared to that when  $s_{ij} = 0, 1$  (Fig. 8). There is still the progressive increase in  $\beta_V$  with age. Both  $\alpha_H$  and  $\phi$  are much different and simply reflect the correlations between the parameters invoked in this

analysis. The fit to the observations (Fig. 12) is basically the same as that obtained in the previous inversions (Table 5). Therefore it has been shown that it is possible to obtain a model which incorporates the *a priori* characteristics of more realistic upper mantle rocks without sacrificing the fit to the observations.



**Figure 11.** Calculated values of the five parameters of the inversion which incorporated the *a priori* correlation between  $\alpha_H$  with  $\beta_V$ , and  $\xi$  with  $\phi$ . The errors are similar to those given in Table 4. The depth resolution is shown in Fig. 10. Note the changes in  $\alpha_H$  and  $\phi$  from that of the previous inversion (Fig. 8) due to the *a priori* constraints imposed by the correlation between parameters.

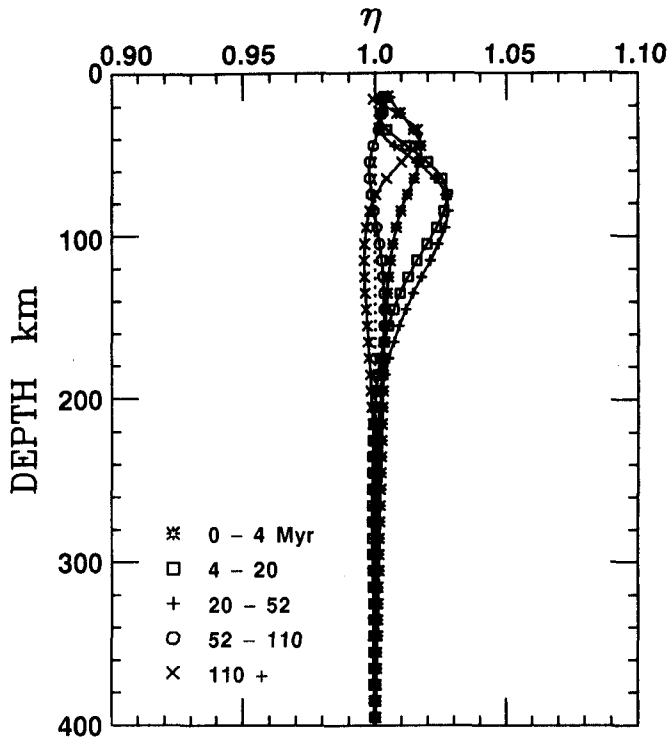


Figure 11. (Continued)

**Effect of attenuation**

Up to this point, we have neglected to include the effect of attenuation on the data. This effect is known to produce a 0.5–1.5 per cent change in the upper mantle structure (Kanamori & Anderson 1977). An attenuation correction is required if one wishes to compare earth models determined from body wave data with those obtained from surface wave or free-oscillation data. Assuming that  $Q_\beta^{-1}$  and  $Q_\alpha^{-1}$  are frequency independent, then the effect of attenuation is given by (Kanamori & Anderson 1977)

$$C(\omega) = C(\omega_r) \left[ 1 + \frac{1}{\pi Q_m(\omega)} \ln \left( \frac{\omega}{\omega_r} \right) \right], \quad (5)$$

where

$\omega$  = angular frequency,

$\omega_r$  = reference angular frequency,

$Q_m(\omega)$  = attenuation factor.

If some model for the attenuation parameters  $Q_\beta$  and  $Q_\alpha$  is known, then  $Q_m(\omega)$  can be computed by (Anderson *et al.* 1965)

$$Q_m^{-1} = \sum_{i=1}^N \left[ \frac{\beta_i}{C} \frac{\partial C}{\partial \beta_i} Q_{\beta_i} + \frac{\alpha_i}{C} \frac{\partial C}{\partial \alpha_i} Q_{\alpha_i}^{-1} \right]. \quad (6)$$

Our illustration of the effect of attenuation uses the Pacific  $Q_\beta^{-1}$  structure of Mitchell, Yacoub & Correig (1977).  $Q_\alpha^{-1}$  is assumed to be twice the magnitude of  $Q_\beta^{-1}$  with the reference frequency chosen to be 1 Hz.

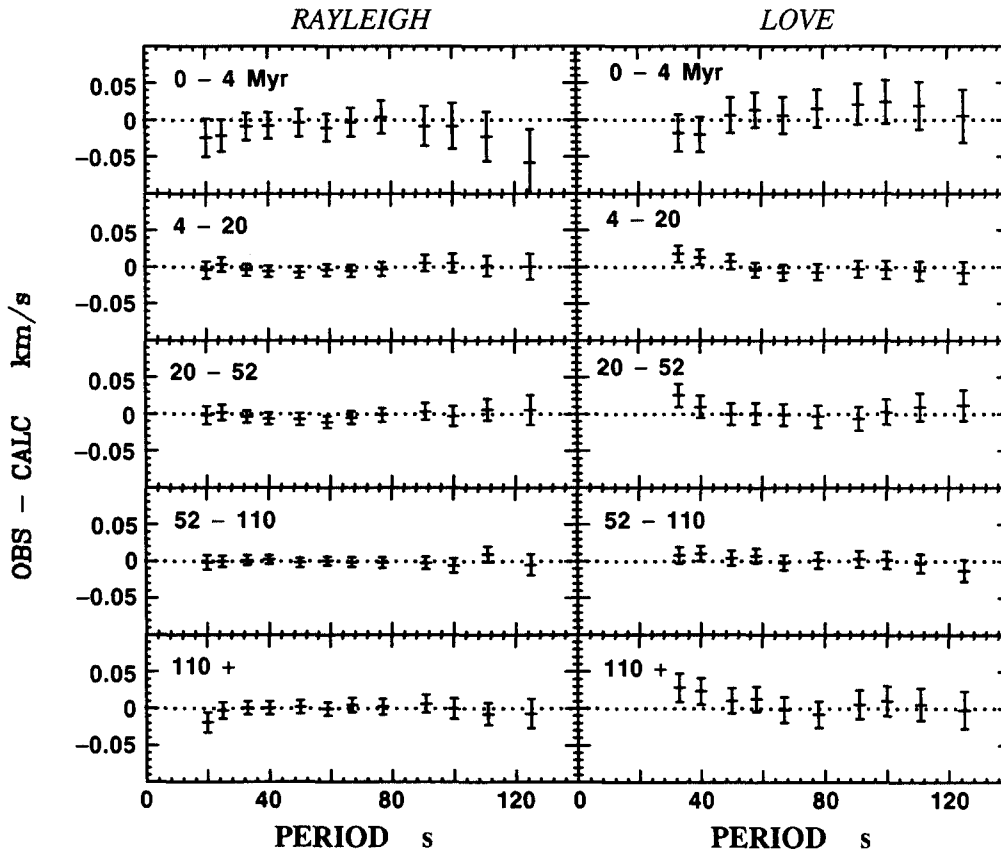


Figure 12. Fit of the model which include the additional non-zero *a priori* correlation coefficients of the parameters (Fig. 11) to the observed pure-path phase velocities. Errors bars are the one sigma variations. Note the similarity to Fig. 9.

**Table 5.** Calculated errors for the inversions for the transverse isotropic upper mantle structure. Top value is the sum of the squares (SSE) of the errors normalized by the associated observational errors. Bottom value is the calculated, non-normalized SSE ( $\text{km s}^{-1}$ ).

Model	Age Region (Myr)				
	0-4	4-20	20-52	52-110	110+
No parameter covariances: (Figure 9)	0.687 0.021	0.656 0.007	0.620 0.009	0.478 0.006	0.635 0.011
Parameter covariances: (Figure 12)	0.601 0.019	0.621 0.007	0.582 0.008	0.442 0.005	0.600 0.011
Attenuation: (not shown)	0.623 0.019	0.485 0.005	0.548 0.008	0.419 0.005	0.551 0.009

Inversions are performed using the *a priori* parameter covariance matrix,  $C_{pp}$ , which incorporated the expected tradeoffs of  $\alpha_H$  with  $\beta_V$ , and  $\xi$  with  $\phi$ . The basic results obtained when the effect of attenuation is included (Fig. 13) are qualitatively similar to those obtained previously; (1) the two most resolvable parameters are  $\beta_V$  and  $\xi$ , (2)  $\beta_V$  progressively increases with age, and (3)  $\xi$  increases rapidly with age until some constant level is reached in regions greater than 20 Myr in age. The primary change of this model is the increase in  $\beta_V$  with respect to the results of the previous inversions, with the largest perturbations centred in the asthenosphere (Fig. 14). The change in this depth region was expected since the amplitude of  $Q^{-1}$  (hence the effect of attenuation) is largest in the asthenosphere. The net result is that the contrast between the velocities in the lithosphere and asthenosphere is smaller. Unfortunately the variation of attenuation with age of the seafloor is not known well enough to incorporate into our models. The

expected effect is a reduction of the magnitude of change in  $\beta_V$  with age, although the general pattern is not expected to change significantly.

This reduction in the difference between the velocities in the lithosphere and asthenosphere when the effect of attenuation is included has little bearing on the results of this study but are significant if one inverts for a discrete model. The smaller contrast in velocity blurs the distinction between the lithosphere and underlying asthenosphere thereby increasing the uncertainty in quantifying the seismic plate thickness. This gives discrete models additional freedom in setting the thickness of the plate.

#### Azimuthal anisotropy

For the case of a complete anisotropic, plane-layered structure, the number of independent elastic parameters increases from 5 to 21. It is fairly obvious that it is not

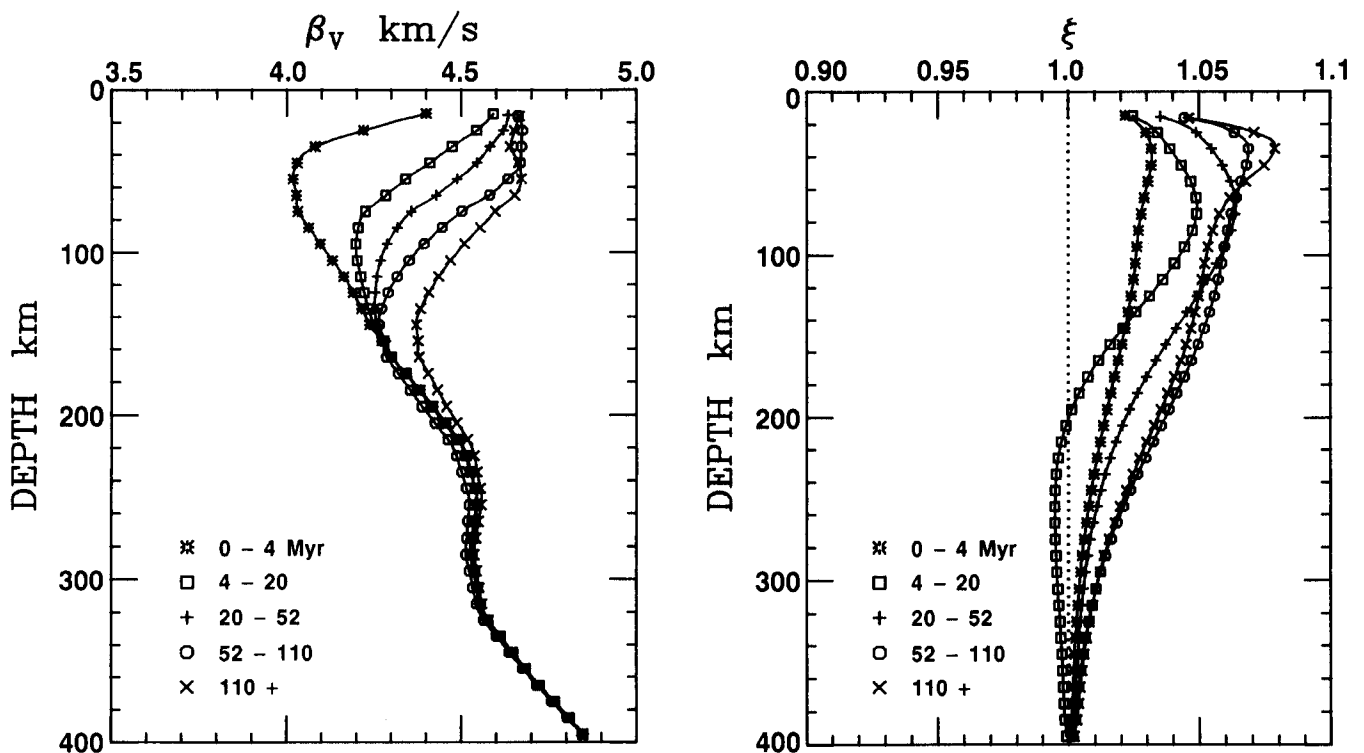


**Figure 13.** Transversely isotropic upper mantle structure calculated when the effect of attenuation is included. Only the two parameters,  $\beta_V$  and  $\xi$ , which describe the shear wave velocities are shown.

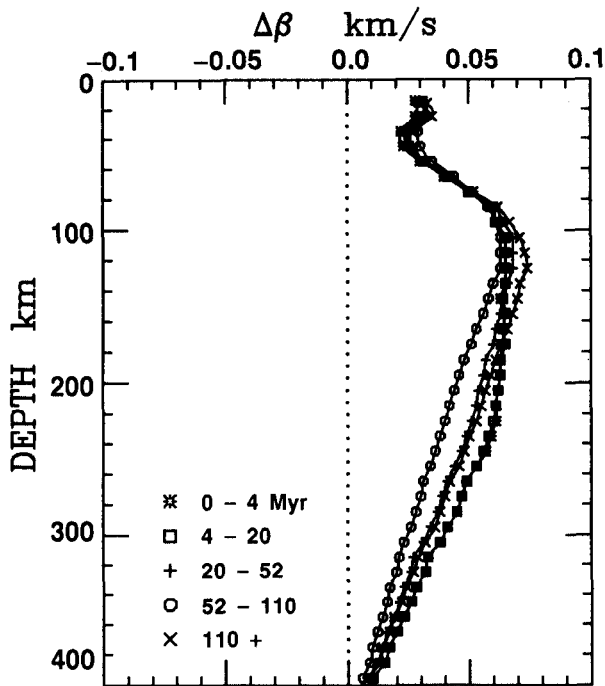


Figure 14. Change in the parameter  $\beta_v$  when attenuation is included as compared to that obtained without this effect (Fig. 11). The largest perturbations are centred in the asthenosphere where the effect of attenuation is the largest.

possible to constrain all the parameters using fundamental-mode surface wave data alone. In order to make this problem feasible, several simplifications must first be made. Smith & Dahlen (1973) have shown that the variation in phase velocity for small degrees of anisotropy can be expressed by

$$C = C_r + C_1 \cos 2\psi + C_2 \sin 2\psi + C_3 \cos 4\psi + C_4 \sin 4\psi, \tag{7}$$

where  $\psi$  is the azimuth between the direction of wave propagation and the angle to some reference pole,  $C_r$  is the reference phase velocity which corresponds to the azimuthally averaged velocity, and the  $C_i$  values are the anisotropic coefficients. In the previous studies (Nishimura & Forsyth, 1985, 1988), we only solved for the  $2\psi$  terms as  $4\psi$  variations were not properly constrained by the path coverage. Love wave azimuthal anisotropy is not statistically required by the data and will hence be neglected. For Rayleigh waves, the  $\sin 2\psi$  terms were close to zero (Table 6) when either a fossil seafloor spreading or a present-day absolute plate motion reference frame was used to calculate the anisotropy coefficients. Zero  $\sin 2\psi$  terms and negative  $\cos 2\psi$  terms correspond to fastest wave propagation in the direction of spreading. The simplified problem in calculating the anisotropic structure is therefore reduced to solving for the anisotropic parameters which are related to the Rayleigh wave  $\cos 2\psi$  term.

Recently, Montagner & Nataf (1986) have proposed a simple means of calculating the partial derivatives required for the inversion of an azimuthal anisotropic structure. This is an approximate method which assumes that the degree of azimuthal anisotropy is small and, more importantly, that the formulation for a flat earth is equally applicable to a structure with spherical symmetry. For the purposes of this study, none of these constraints are unrealistic.

First, the application of an approximate method is in accord with the resolution inherent in azimuthal anisotropy calculations. Precise measurements of this second-order effect are difficult to make as one must also take into account other perturbations, such as lateral variations in structure. It is expected that the errors in the data (noise and modelling imperfections) far exceed the imprecision of the analytical method. Finally, there is still some ambiguity concerning the tectonic history of the western Pacific and, hence, there are possible errors in the fossil seafloor spreading map used in deriving the azimuthal coefficients that may contribute to inaccuracies in the calculation of the coefficients primarily in the oldest age region.

Table 6. Rayleigh wave azimuthal anisotropy coefficients (top) and one sigma errors (bottom).

	PERIOD (s)											
	20.0	25.0	33.3	40.0	50.0	58.8	66.7	76.9	90.9	100.0	111.1	125.0
COS2 $\psi$	-0.00850	-0.00869	-0.00913	-0.00968	-0.01032	-0.00991	-0.00988	-0.00959	-0.00988	-0.00858	-0.00598	-0.00513
	0.00138	0.00117	0.00101	0.00096	0.00096	0.00094	0.00101	0.00109	0.00127	0.00149	0.00161	0.00213
SIN2 $\psi$	-0.00273	-0.00276	-0.00304	-0.00238	-0.00210	-0.00231	-0.00242	-0.00138	-0.00089	0.00065	0.00199	0.00216
	0.00133	0.00114	0.00099	0.00094	0.00094	0.00094	0.00099	0.00107	0.00126	0.00141	0.00151	0.00201
FOSSIL SEAFLOOR SPREADING AGE < 80 Myr												
COS2 $\psi$	-0.00866	-0.00543	-0.00364	-0.00241	-0.00135	-0.00093	0.00064	0.00128	0.00004	-0.00146	-0.00138	-0.00120
	0.00307	0.00225	0.00180	0.00171	0.00172	0.00168	0.00177	0.00192	0.00222	0.00245	0.00260	0.00329
SIN2 $\psi$	0.00669	0.00288	0.00397	0.00291	0.00398	0.00413	0.00283	0.00168	-0.00199	-0.00299	-0.00268	0.00034
	0.00300	0.00223	0.00190	0.00181	0.00182	0.00178	0.00189	0.00204	0.00230	0.00263	0.00289	0.00366
FOSSIL SEAFLOOR SPREADING AGE > 80 Myr												
COS2 $\psi$	-0.00637	-0.00622	-0.00671	-0.00714	-0.00745	-0.00761	-0.00797	-0.00729	-0.00815	-0.00727	-0.00486	-0.00404
	0.00130	0.00107	0.00094	0.00089	0.00091	0.00087	0.00089	0.00096	0.00107	0.00115	0.00127	0.00172
SIN2 $\psi$	0.00275	0.00237	0.00167	0.00176	0.00159	0.00121	0.00059	0.00110	0.00170	0.00216	0.00299	0.00341
	0.00122	0.00107	0.00093	0.00088	0.00090	0.00086	0.00088	0.00095	0.00109	0.00125	0.00132	0.00172
PRESENT-DAY ABSOLUTE PLATE MOTION AGE < 80 Myr												

The basic method of Montagner & Nataf (1986) which is applicable to the simplified problem can be briefly summarized here. For a plane layered structure, the perturbation in Rayleigh wave phase velocity related to the  $\cos 2\psi$  terms is given by (using the notation of Takeuchi & Saito 1972)

$$\delta C(k) = \frac{1}{2C(k)} R_2(k) \cos 2\psi$$

$$R_2(k) = \frac{1}{I_1} \int_0^\infty \left[ B_c y_1^2 + H_c \frac{2y_1 y_3}{k} + G_c \left( \frac{y_3'}{k} - y_1 \right)^2 \right] dz, \quad (8)$$

where  $y_1$  and  $y_3$  are the Rayleigh wave displacement functions,  $y_1'$  and  $y_3'$  are the derivative of  $y_1$  and  $y_3$  with respect to depth,  $k$  is the wave number,  $I_1$  is the energy integral, and  $B_c$ ,  $H_c$  and  $G_c$  are the anisotropic parameters of the problem (Appendix). In this case, the partial derivatives with respect to  $B_c$ ,  $H_c$  and  $G_c$  are equivalent to the derivatives with respect to  $\alpha_H$ ,  $\xi$  and  $\beta_V$ .

Inversions were performed using a correlation length,  $\Delta$ , of 10 km with a starting model of  $G_c = B_c = H_c = 0$ . The standard deviations of the *a priori* parameter covariances matrix,  $C_{pp}$ , were set equal to 0.005 mbar with  $s_{ij} = 0$  except when the  $i$ th and  $j$ th parameters are the same type (then  $s_{ij} = 1$ ). The resultant structure ( $G_c$ ,  $B_c$  and  $H_c$ ) was calculated using the azimuthal anisotropy  $\cos 2\psi$  coefficients obtained using the relative plate motion reference frame in regions of age less than 80 Myr. In Fig. 15 we only present the results for  $G_c$  along with the associated  $1\sigma$  errors; the

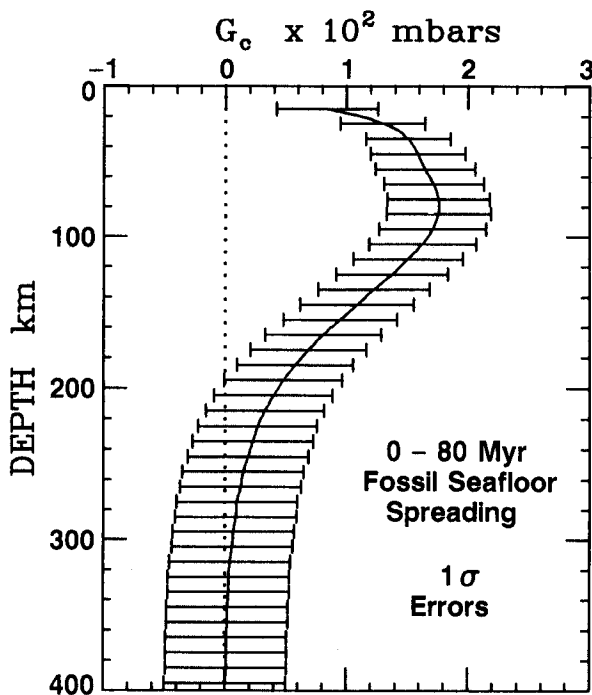


**Figure 15.** Azimuthal anisotropy parameter,  $G_c$ , computed for inversions for fossil seafloor spreading direction in regions younger than 80 Myr. Errors are the one sigma values obtained from the *a posteriori* parameter covariance matrix. Azimuthal anisotropy extends down to depths below the base of the lithosphere and represents the contributing effect of anisotropy in both the lithosphere (related to fossil seafloor spreading) and the asthenosphere (related to absolute plate motion).

computed  $B_c$  and  $H_c$  parameters were essentially zero. The dominance of  $G_c$  was expected as the derivatives associated with this parameter are the same as that for  $\beta_V$  (the dominant Rayleigh wave parameter for a transversely isotropic structure). We therefore will use the results for  $G_c$  when interpreting the results of this analysis. However, one must keep in mind that shallow level anisotropy related to the  $B_c$  terms can have an effect on the  $\cos 2\psi$  coefficients (Montagner & Nataf 1986). The contribution of shallow level, non-zero  $B_c$  diminishes the amplitude of  $G_c$  but this effect is predominantly seen at a period range beyond that of this study.

The computed model indicates that the azimuthal anisotropy effect extends down approximately 200 km with a maximum value at around 75 km (Fig. 15); the largest effect is therefore below the base of the lithosphere (based on thermal models) in the 0–80 Myr region. However, the anisotropy coefficients used in this inversion were calculated using a model (fossil seafloor spreading direction) which should be only applicable to the structure present in the oceanic plate or in the immediate vicinity of mid-ocean ridges; i.e. the azimuthal anisotropic structure should only extend down to the base of the lithosphere. This dilemma is easily reconciled when one considers a potential source of deeper seated azimuthal anisotropy. It was pointed out in a previous study (Nishimura & Forsyth, 1988) that the direction of present-day absolute plate motion is very similar to that of fossil seafloor spreading in the younger regions of the Pacific (Fig. 16). As absolute motion may be indicative of the flow direction (i.e. azimuthal anisotropy) below the oceanic plate, the similarity between the two tectonic models would indicate that the azimuthal anisotropic fabric in regions less than 80 Myr in age will be fairly uniform with depth in this region. Thus our preferred model; shallow azimuthal anisotropy in regions of the Pacific less than 80 Myr in age is related to the direction of fossil seafloor spreading while deeper anisotropy is related to present-day absolute plate motion.

This is further illustrated by the results obtained for the older regions of the Pacific. Azimuthal anisotropy ( $G_c$ ), using the fossil seafloor spreading reference frame, is only non-zero at depths less than 50 km (Fig. 17). One possible explanation for this result is that the azimuthal anisotropic structure at depth below 50 km is equal to zero. We feel that this is unlikely since there is well developed transverse isotropy in the older regions of the Pacific which extends down to 200 km. Instead, the apparent zero value anisotropic structure below 50 km may be due to changes in the orientation of the azimuthal anisotropic fabric with depth. Unlike the younger regions of the Pacific, there are significant differences in the direction of absolute plate motion and fossil seafloor spreading in a large percentage of the western Pacific (Fig. 16). When the two directions are aligned, the contributions of the shallow and the deeper anisotropy may constructively interfere. When the two patterns are different, there may be a destructive interference effect and, therefore, the longer period Rayleigh waves, which are sensitive to a broader range of depths and structures, might be unable to detect azimuthal anisotropy. We would like to be able to model the evolution with age of azimuthal anisotropy in the same detail as the transverse isotropy and  $\beta_V$ . Unfortunately, the tradeoffs between

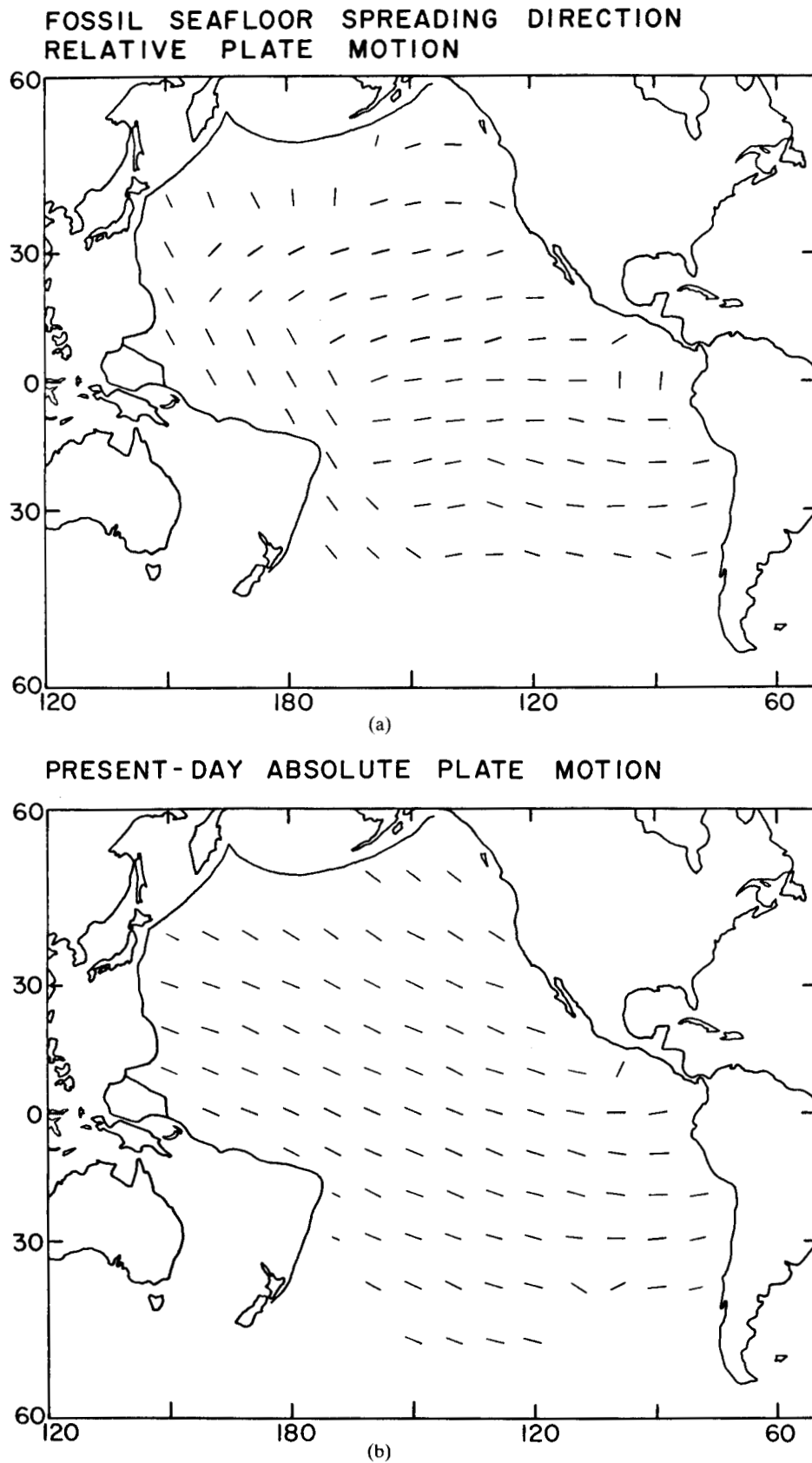


**Figure 16.** The directions of (a) fossil seafloor spreading and (b) present-day absolute plate motion in the Pacific. There is a good overall correlation in the orientation of the two models in the younger regions. In the western Pacific, the two patterns are divergent over much of this region.

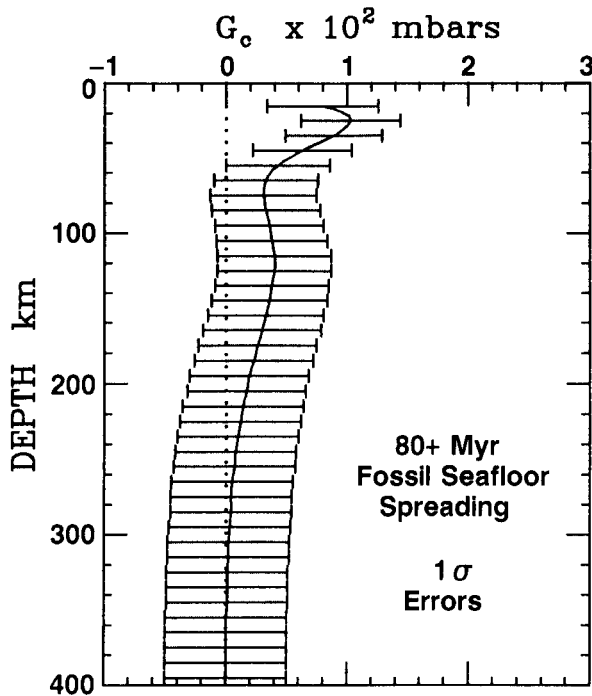


**Figure 17.** Azimuthal anisotropy parameter,  $G_c$ , computed for inversions for fossil seafloor spreading direction in regions older than 80 Myr. Errors are the one sigma, *a posteriori* values. The apparent lack of anisotropy below 50 km may be due to differences in the anisotropic fabric in the lithosphere and asthenosphere; differences with depth results in destructive interference.

azimuthal anisotropic velocities and laterally heterogeneities prevents comparable horizontal resolution of the azimuthal terms.

## DISCUSSION

The depth extent and pattern of both transverse and azimuthal anisotropy leads us to believe that the two types of anisotropy share a common origin. A viable mechanism which can produce this total anisotropic structure is the preferred alignment of olivine, a mineral ubiquitous in the oceanic upper mantle (Fig. 18). Olivine is an orthorhombic mineral which is characterized by major differences in the elastic properties of its *a*-, *b*- and *c*-axes (Kumazawa & Anderson 1969). The dominant factor which controls the amplitude and orientation of anisotropy is the alignment of the *a*-axis; the elastic parameters associated with the *a*-axis [100] (fastest velocities) are much different from those associated with both the *b*- or *c*-axes.

Supporting evidence for the importance of olivine is provided by laboratory measurements of the elastic properties of ultramafic rocks from ophiolite sequences (Christensen 1984). The degree of anisotropy was found to be dependent on the percentage of olivine present. Rocks with a higher abundance of minerals other than olivine (e.g. orthopyroxene) displayed less anisotropy. The amplitude of the transversely and azimuthally anisotropic effect can vary widely depending on the abundance and preferred orientation of olivine. In ultramafic rocks derived from ophiolite sequences, olivine is found to be aligned with an

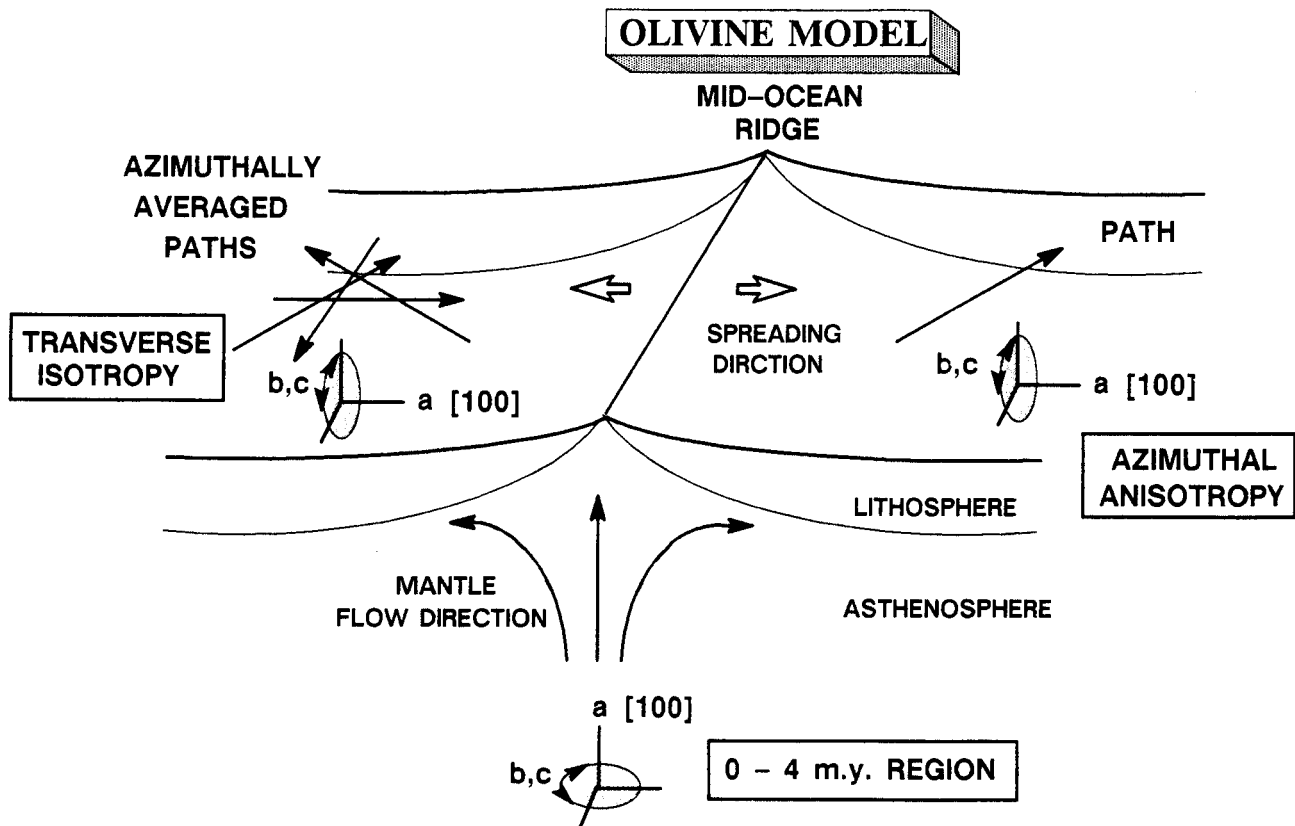


**Figure 18.** Idealized schematic diagram illustrating the preferred model for the oceanic upper mantle in the Pacific. The transversely isotropic effect is due to the averaging of the azimuthally dependent velocities in an upper mantle containing horizontally aligned olivine over the entire range of azimuths. The low amplitude of the transverse isotropic effect under the mid-ocean ridge system (0–4 Myr age zone) as illustrated by the  $\xi$  terms of Figs 8 & 11, and 13, is due to the contribution of both horizontal and vertical flow in the upper mantle in this age region.

orientation of the  $a$ -axis (fastest velocities) parallel to the inferred direction of fossil seafloor spreading (Peselnick & Nicolas 1978; Christensen & Salisbury 1979; Christensen 1984).

In order to produce both the transverse and azimuthal anisotropy, the olivine  $a$ -axis must be preferentially aligned in the horizontal plane. In our preferred model this systematic orientation is the direction of fossil seafloor spreading at shallow mantle depths, and the direction of absolute plate motion at sub-lithospheric depths. As pointed

out by Crampin (1977), it is not possible to determine whether or not the olivine  $b$ - or  $c$ -axes are systematically oriented; the elastic properties associated with these axes are quite similar. This systematic alignment is equivalent to a hexagonal system with a horizontal axis of symmetry.

It should be noted that the preferential alignment of olivine crystals in the direction of mantle flow helps to explain the results obtained for the youngest region of the Pacific (0–4 Myr). Theoretical models have shown that beneath mid-ocean ridges, the dominant mantle flow

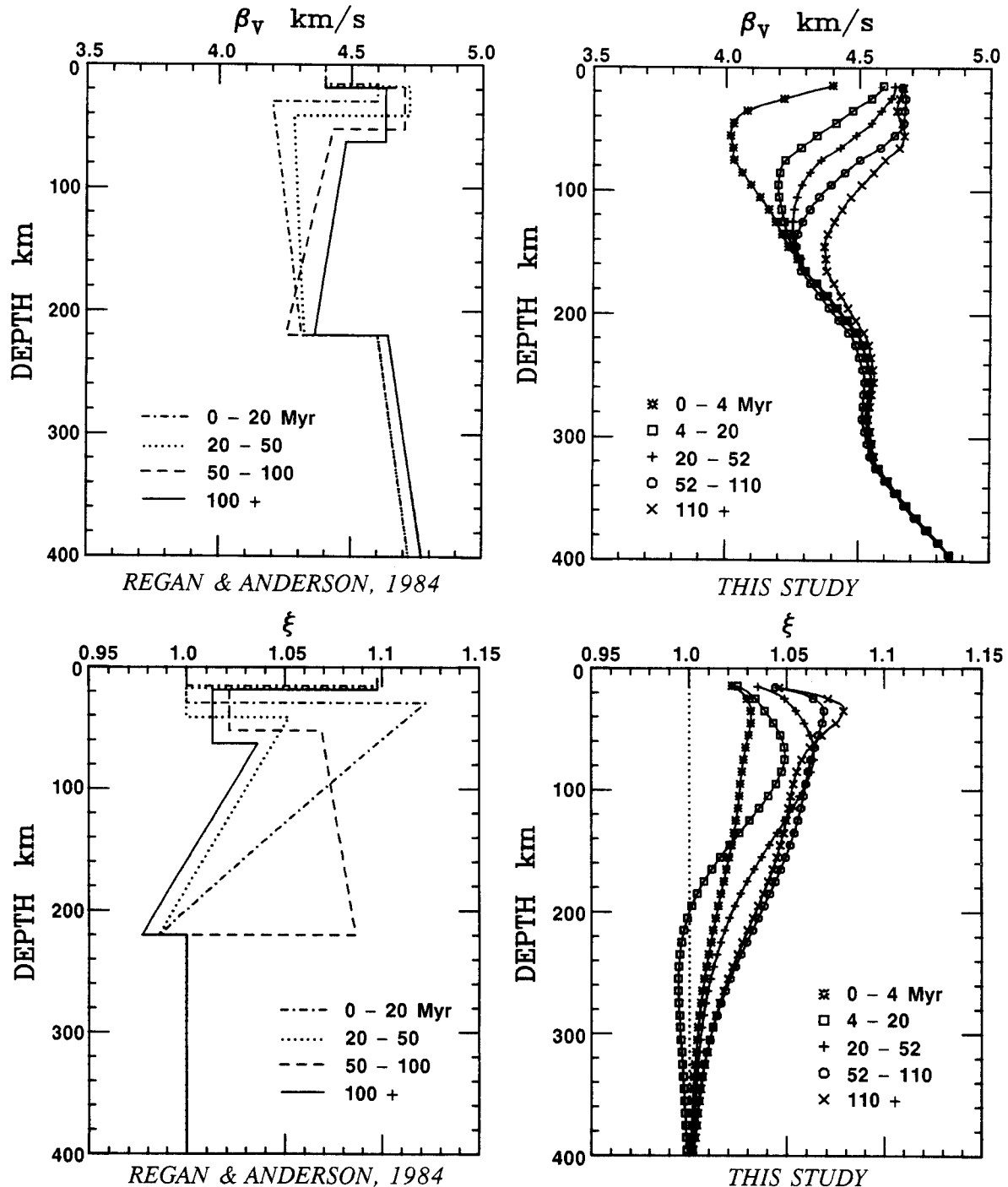


**Figure 19.** Comparison of the velocity-age model of Regan & Anderson (1984) and that of this study. Shown are the most resolvable parameters,  $\beta_V$  and  $\xi$  (computed from the  $\beta_H$  terms of Regan & Anderson).



direction is vertical as opposed to a more horizontal orientation away from the ridges (e.g. Phipps Morgan & Forsyth 1988) and, therefore, the transverse anisotropy effect in the youngest region should be different from that observed for the older regions. Our results indicate that the only resolvable anisotropic parameter,  $\xi$ , is smallest in this age zone, with  $\xi$  rapidly increasing to some apparent equilibrium level in the older regions. Therefore, for this youngest region, the lower values for  $\xi$  may be due to a combination of the vertical and horizontal flow direction beneath the mid-ocean ridges.

Finally, it should be noted that the requirement that the variations from one age zone to the next be minimized contrasts dramatically with the results of some recently computed models for the age dependent oceanic upper mantle velocity structure (Regan & Anderson 1984; Kawasaki 1986). These models have proposed that there is a correspondence between the seismic and mechanical lithospheric thickness with the base of the overlying plate correlating with the depth of the theoretical 600°C isotherm. However, these velocity profiles cannot be representative of some *simple* age dependence as the computed velocity structures change dramatically from one age province to the next (e.g. Regan & Anderson; Fig. 19). We implicitly assume that when pure-path velocities have a simple age dependence, the computed velocity structures should also have a simple age dependence.

The primary reasons why the results of Regan & Anderson, and Kawasaki differ from that of this study are the differences in the modelling philosophy and procedure, and differences in data. In this study, we purposely overparameterize the inverse problem by using a large number of thin layers when modelling for the velocity structure. The application of a robust inversion technique (Tarantola & Valette 1982) allows the inverse problem to be solved stably; the computed velocity models of this study are a better representation of the true resolving power of the constraining fundamental-mode surface wave data set. In the case of Regan & Anderson, and Kawasaki, a more *ad hoc forward* modelling procedure was used with the depth dependent model parameterized by a limited number of parameters (e.g. constant velocity gradients). This can produce rather unusual velocity models (Fig. 19); i.e. a large seismic discontinuity at 220 km depth, large variations in  $\xi$  with age, and sharp discontinuities in  $\xi$  with depth. The pure-path data set used in these studies (Mitchell & Yu 1980) employed fewer paths with larger observational errors and did not yield a simple monotonic increase in phase velocity as a function of age of the seafloor.

## CONCLUSIONS

The basic conclusions of this study can be summarized as follows.

(1) The structure of the upper mantle in the Pacific varies smoothly as a function of the age of the seafloor. The primary resolvable parameter for a transversely isotropic medium,  $\beta_V$ , progressively increases as a function of age and qualitatively mimics the temperature structure calculated by thermal models of the cooling of the oceanic plate. The greatest change in velocity occurs within the first 20 Myr.

(2) The upper mantle down to 200 km depth is characterized by a significant degree of transverse anisotropy. The shear wave anisotropy term,  $\xi$ , which is the only resolvable parameter other than  $\beta_V$ , rapidly increases in magnitude in the first 20 Myr until some equilibrium value is reached beyond this age.

(3) The azimuthal anisotropic structure in regions less than 80 Myr in age, when constrained by the fossil seafloor spreading reference frame, reaches a maximum value between 25 and 100 km depth and is present down to 200 km.

(4) In the older regions of the Pacific (greater than 80 Myr in age), azimuthal anisotropy is confined to a much shallower depth (50 km). The apparent decrease in azimuthal anisotropy in the western Pacific may be due to the variations in the horizontal direction of anisotropic fabric with depth rather than a decrease in *in situ* anisotropy.

(5) The depth extent and magnitude of both transverse and azimuthal anisotropy can be explained by an upper mantle which contains olivine with preferred orientations.

## ACKNOWLEDGMENTS

We thank the many people who provided preprints of their work, especially J. Leveque, J. Montagner and H. C. Nataf. We especially thank Peter Shearer who did an extremely thorough job of reviewing this paper. This work was sponsored by the National Science Foundation under contract EAR83-13170.

## REFERENCES

- Anderson, D. L., 1961. Elastic wave propagation in layered anisotropic media, *J. geophys. Res.*, **66**, 2953-2963.
- Anderson, D. L., 1966. Recent evidence concerning the structure and composition of the Earth's mantle, *Phys. Chem. Earth*, **6**, 1-131.
- Anderson, D. L. & Dziewonski, A. M., 1982. Upper mantle anisotropy: evidence from free oscillations, *Geophys. J. R. astr. Soc.*, **69**, 383-404.
- Anderson, D. L., Ben-Menahem, A. & Archambeau, C. B., 1965. Attenuation of seismic energy in the upper mantle, *J. geophys. Res.*, **70**, 1441-1448.
- Backus, G. & Gilbert, F., 1968. The resolving power of gross earth data, *Geophys. J. R. astr. Soc.*, **16**, 169-205.
- Boore, D. M., 1969. Effect of higher mode contamination on measured Love wave phase velocities, *J. geophys. Res.*, **74**, 6612-6616.
- Cara, M., 1979. Lateral variations of *S* velocity in upper mantle from higher Rayleigh modes, *Geophys. J. R. astr. Soc.*, **57**, 649-670.
- Cara, M. & Leveque, J. J., 1987. Oriented olivine crystals in the upper mantle: a test from the inversion of multimode surface-wave data, *Phys. Earth planet. Int.*, **47**, 246-252.
- Christensen, N. I., 1984. The magnitude, symmetry and origin of upper mantle anisotropy based on fabric analyses of ultramafic tectonites, *Geophys. J. R. astr. Soc.*, **76**, 89-111.
- Christensen, N. I. & Salisbury, M. H., 1979. Seismic anisotropy in the oceanic upper mantle: evidence from the Bay of Islands ophiolite complex, *J. geophys. Res.*, **84**, 4601-4610.
- Crampin, S., 1977. A review of the effects of anisotropic layering on the propagation of seismic waves, *Geophys. J. R. astr. Soc.*, **49**, 9-27.
- Crampin, S., 1984. An introduction to wave propagation in anisotropic media, *Geophys. J. R. astr. Soc.*, **76**, 17-28.
- Crough, S. T., 1978. Thermal origin of mid-plate hot-spot swells, *Geophys. J. R. astr. Soc.*, **55**, 451-469.

- Estey, L. H. & Douglas, B. J., 1986. Upper mantle anisotropy: a preliminary model, *J. geophys. Res.*, **91**, 11393–11406.
- Forsyth, D. W., 1975. The early structural evolution and anisotropy of the oceanic upper mantle, *Geophys. J. R. astr. Soc.*, **43**, 103–162.
- Francis, T. J. G., 1969. Generation of seismic anisotropy along the mid-oceanic ridges, *Nature*, **221**, 162–165.
- Fuchs, K., 1977. Seismic anisotropy of the subcrustal lithosphere as evidence for dynamical processes in the upper mantle, *Geophys. J. R. astr. Soc.*, **49**, 167–179.
- Hess, H. H., 1964. Seismic anisotropy of the uppermost mantle under oceans, *Nature*, **203**, 629–631.
- Journet, B. & Jobert, N., 1982. Variations with age of anisotropy under oceans, from great circle surface waves, *Geophys. Res. Lett.*, **9**, 179–181.
- Kanamori, H. & Anderson, D. L., 1977. Importance of physical dispersion in surface wave and free oscillation problems: *Review, Rev. Geophys. Space Phys.*, **15**, 105–112.
- Kawasaki, I., 1986. Azimuthally anisotropic model of the oceanic upper mantle, *Phys. Earth planet. Int.*, **43**, 1–21.
- Keen, C. E. & Barrett, D. L., 1971. A measurement of seismic anisotropy in the northeast Pacific, *Can. J. Earth Sci.*, **8**, 1056–1076.
- Kirkwood, S. C. & Crampin, S., 1981. Surface-wave propagation in an ocean basin with an anisotropic upper mantle: observations of polarization anomalies, *Geophys. J. R. astr. Soc.*, **64**, 487–497.
- Knopoff, L. & Chang, F. S., 1977. The inversion of surface wave dispersion data with random errors, *J. Geophys.*, **43**, 299–309.
- Kumazawa, M. & Anderson, O. L., 1969. Elastic moduli, pressure derivatives and temperature derivatives of single crystal olivine and single crystal forsterite, *J. geophys. Res.*, **74**, 5961–5971.
- Kuo, B. Y., Forsyth, D. W. & Wyssession, M., 1987. Lateral heterogeneity and azimuthal anisotropy in the north Atlantic determined from SS–S differential travel times, *J. geophys. Res.*, **92**, 6421–6436.
- Lerner-Lam, A. & Jordan, T. H., 1983. Earth structure from fundamental and higher mode waveform analysis, *Geophys. J. R. astr. Soc.*, **75**, 754–798.
- Leveque, J. J. & Cara, M., 1983. Long-period Love wave overtone data in North America and the Pacific Ocean: new evidence for upper mantle anisotropy, *Phys. Earth planet. Int.*, **33**, 164–179.
- Leveque, J. J. & Cara, M., 1985. Inversion of multimode surface wave data: evidence for sub-lithospheric anisotropy, *Geophys. J. R. astr. Soc.*, **83**, 753–773.
- Love, A. E. H., 1927. *A Treatise on the Mathematical Theory of Elasticity*, Cambridge University Press, Cambridge.
- Maupin, V., 1985. Partial derivatives of surface wave phase velocities for flat anisotropic models, *Geophys. J. R. astr. Soc.*, **83**, 379–398.
- McNutt, M. K., 1984. Lithospheric flexure and thermal anomalies, *J. geophys. Res.*, **89**, 11180–11194.
- Mitchell, B. J., Yacoub, N. & Correig, A., 1977. A summary of seismic surface wave attenuation and its regional variation across the continents and oceans, in *The Earth's Crust, its Nature and Physical Properties*, *Geophys. Monograph 20*, pp. 405–425, ed. Heacock, J., American Geophysical Union, Washington, DC.
- Mitchell, B. J. & Yu, G. K., 1980. Surface wave dispersion, regionalized velocity models, and anisotropy of the Pacific crust and upper mantle, *Geophys. J. R. astr. Soc.*, **63**, 497–514.
- Montagner, J. P., 1985. Seismic anisotropy of the Pacific inferred from long-period surface waves dispersion, *Phys. Earth planet. Int.*, **38**, 28–50.
- Montagner, J. P. & Jobert, N., 1981. Investigation of upper mantle structure under young regions of the southeast Pacific using long-period Rayleigh waves, *Phys. Earth planet. Int.*, **27**, 206–222.
- Montagner, J. P. & Nataf, H. C., 1986. On the inversion of the azimuthal anisotropy of surface waves, *J. geophys. Res.*, **91**, 511–520.
- Nataf, H. C., Nakanishi, I. & Anderson, D. L., 1986. Measurements of mantle wave velocities and inversion for lateral heterogeneities and anisotropy, Part III: Inversion, *J. geophys. Res.*, **91**, 7261–7307.
- Nishimura, C. E. & Forsyth, D. W., 1985. Anomalous Love-wave phase velocities in the Pacific: sequential pure-path and spherical harmonic inversion, *Geophys. J. R. astr. Soc.*, **81**, 389–407.
- Nishimura, C. E. & Forsyth, D. W., 1988. Rayleigh wave phase velocities in the Pacific with implications for azimuthal anisotropy and lateral heterogeneities, *Geophys. J. R. astr. Soc.*, **94**, 479–501.
- Okal, E. A. & Talandier, J., 1980. Rayleigh-wave phase velocities in French Polynesia, *Geophys. J. R. astr. Soc.*, **63**, 719–733.
- Parker, R. L. & Oldenburg, D. W., 1973. A thermal model of oceanic ridges, *Nature*, **242**, 137–139.
- Parsons, B. & Sclater, J. G., 1977. An analysis of the variation of ocean floor bathymetry and heat flow with age, *J. geophys. Res.*, **82**, 803–827.
- Peselnick, L. & Nicolas, A., 1978. Seismic anisotropy in an ophiolite peridotite: application to oceanic upper mantle, *J. geophys. Res.*, **83**, 1227–1235.
- Phipps Morgan, J. & Forsyth, D. W., 1988. 3-D flow and temperature perturbations due to a transform offset: Effects on oceanic and mantle structure, *J. geophys. Res.*, **93**, 1959–1966.
- Raitt, R. W., Shor, G. G., Francis, T. J. G. & Morris, G. B., 1969. Anisotropy of the Pacific upper mantle, *J. geophys. Res.*, **74**, 3095–3109.
- Regan, J. & Anderson, D. L., 1984. Anisotropic models of the upper mantle, *Phys. Earth Planet. Int.*, **35**, 227–263.
- Schlue, J. W. & Knopoff, L., 1977. Shear-wave polarization anisotropy in the Pacific Basin, *Geophys. J. R. astr. Soc.*, **49**, 145–165.
- Sclater, J. G., Anderson, R. N. & Bell, M. L., 1971. Elevation of ridges and evolution of the central eastern Pacific, *J. geophys. Res.*, **76**, 7888–7915.
- Sclater, J. G., Parsons, B. & Jaupart, C., 1981. Oceans and continents: similarities and differences in the mechanisms of heat loss, *J. geophys. Res.*, **86**, 11535–11552.
- Shearer, P. & Orcutt, J., 1985. Anisotropy in the oceanic lithosphere—theory and observations from the Ngendei seismic refraction experiment in the south-west Pacific, *Geophys. J. R. astr. Soc.*, **80**, 493–526.
- Shearer, P. M. & Orcutt, J. A., 1986. Compressional and shear wave anisotropy in the oceanic lithosphere—the Ngendei seismic refraction experiment, *Geophys. J. R. astr. Soc.*, **87**, 967–1003.
- Shimamura, H., 1984. Anisotropy in the oceanic lithosphere of the northwestern Pacific basin, *Geophys. J. R. astr. Soc.*, **76**, 253–260.
- Shimamura, H. & Asada, T., 1983. Velocity anisotropy extending over the entire depth of the oceanic lithosphere, in *Final Report of the International Geodynamics Program*, pp. 121–125, Geodynamics Series (Working Group 1), ed. Hilde, T. W. C., American Geophysical Union, Washington, DC.
- Smith, M. L. & Dahlen, F. A., 1973. The azimuthal dependence of Love and Rayleigh wave propagation in a slightly anisotropic medium, *J. geophys. Res.*, **78**, 3321–3333.
- Suetsugu, D. & Nakanishi, I., 1987. Regional and azimuthal dependence of phase velocities of mantle Rayleigh waves in the Pacific Ocean, *Phys. Earth planet. Int.*, **47**, 230–245.
- Takeuchi, H. & Saito, M., 1972. Seismic surface waves, in *Methods in Computational Physics*, vol. 11, pp. 217–295, Academic Press, New York.
- Tanimoto, T., 1986. The Backus–Gilbert approach to the 3-D structure in the upper mantle—II. SH and SV velocity, *Geophys. J. R. astr. Soc.*, **84**, 49–69.
- Tanimoto, T. & Anderson, D. L., 1985. Lateral heterogeneity and azimuthal anisotropy of the upper mantle: Love and Rayleigh waves 100–250 s, *J. geophys. Res.*, **90**, 1842–1858.
- Tarantola, A. & Valette, B., 1982. Generalized nonlinear inverse problems solved using the least squares criterion, *Rev. Geophys. Space Phys.*, **20**, 219–232.
- Wielandt, E. & Knopoff, L., 1982. Dispersion of very long-period Rayleigh waves along the East Pacific Rise: Evidence for S wave velocity anomalies to 450 km depth, *J. geophys. Res.*, **87**, 8631–8641.
- Wiggins, R. A., 1972. The general linear inverse problem: Implications of surface waves and free oscillations for earth structure, *Rev. Geophys. Space Phys.*, **10**, 251–285.
- Woodhouse, J. H. & Dziewonski, A. M., 1984. Mapping the upper

mantle: three-dimensional modeling of earth structure by inversion of seismic waveforms, *J. geophys. Res.*, **89**, 5953–5986.

Yoshida, M., 1983. Surface wave polarization anisotropy in the west Pacific revealed from group velocities and synthetic waves, *Bull. Earthq. Res. Inst.*, **58**, 571–589.

Yoshida, M., 1984. Surface wave polarization anisotropy near the East Pacific Rise as revealed from group velocities and synthetic waves, *Bull. Earthq. Res. Inst.*, **59**, 383–398.

Yu, G. K. & Mitchell, B. J., 1979. Regionalized shear velocity models of the Pacific upper mantle from observed Love and Rayleigh wave dispersion, *Geophys. J. R. astr. Soc.*, **57**, 311–341.

## APPENDIX

The properties of a transversely isotropic structure with a vertical axis of symmetry can be represented by five independent elastic parameters. In the notation of Love (1927), the elastic coefficients are given by  $A$ ,  $L$ ,  $N$ ,  $C$  and  $F$ , where

$$A = \rho\alpha_H^2 = \frac{3}{8}(C_{11} + C_{22}) + \frac{1}{4}C_{12} + \frac{1}{2}C_{66}$$

$$L = \rho\beta_V^2 = \frac{1}{2}(C_{44} + C_{55})$$

$$N = \rho\beta_H^2 = \frac{1}{8}(C_{11} + C_{22}) - \frac{1}{4}C_{12} + \frac{1}{2}C_{66}$$

$$C = \rho\alpha_V^2 = C_{33}$$

$$F = \text{fifth elastic parameter} = \frac{1}{2}(C_{13} + C_{23}),$$

$\alpha$  and  $\beta$  are the compressional and shear wave velocities, respectively, in the horizontal (H) and vertical (V) orientations, and  $\rho$  is the density. The  $C_{ij}$  values are the components of the elastic tensor (e.g. Montagner & Nataf 1986). Conversely, the transversely isotropic structure can also be expressed by  $\beta_V$ ,  $\alpha_H$ ,  $\xi$ ,  $\phi$ , and  $\eta$ , where

$$\xi = \frac{N}{L} = \left(\frac{\beta_H}{\beta_V}\right)^2$$

$$\phi = \frac{C}{A} = \left(\frac{\alpha_V}{\alpha_H}\right)^2$$

$$\eta = \frac{F}{A - 2L}.$$

The parameters which describe the azimuthal anisotropic model used in this study are given by three coefficients

$$B_c = \frac{1}{2}(C_{11} - C_{22})$$

$$H_c = \frac{1}{2}(C_{13} - C_{23})$$

$$G_c = \frac{1}{2}(C_{55} - C_{44}).$$